REFERENCES

[1] M. S. Dresselhaus, G. Chen, M. Y. Tang, R. Yang, H. Lee, D. Wang, Z. Ren, J. P. Fleurial and P. Gogna, "New direction for low-dimensional Thermoelectric materials", Advanced materials, 19 (2007) 1043-1053.

[2] A. J. Minnich, M. S. Dresselhaus, Z. F. Ren and G. Chen, "Bulk nanostructureed thermoelectric materials: current research and future prospects", *Energy & Environmental Science*, 2 (2009) 466-479.

[3] T. M. Tritt and M. A. Subramanian, "Thermoelectric materials, phenomena, and applications: a bird's eye view", *MRS Bull.*, 31 (2006) 188-198.

[4] L. E. Bell, "Cooling, heating, generating power, and recovering waste heat with thermoelectric systems", *Science*, 321 (2008) 1457-1461.

[5] D. M. Rowe, *CRC Handbook of Thermoelectrics*, CRC Press, New York, (1995).

[6] C. Uher, *Thermoelectrics handbook: Macro to Nano*, edited by D. M. Rowe, Taylor and Francis, CRC, Boca Raton, FL (2006) 34-1-34-17.

[7] K. F. Hsu, S. Loo, F. Guo, W. Chen, J. S. Dyck, C. Uher, T. Hogan, E. K. Polychroniadis, M. G. Kanatzidis, "Cubic $AgPb_mSbTe_{2+m}$: Bulk thermoelectric materials with high figure of merit", *Science*, 303 (2004) 818-821.

[8] G. J. Snyder and E. S. Toberer, "Complex thermoelectric materials" *Nat. Mater.*, 7 (2008) 105-113.

[9] S. Bhunia and D. N. Bose, "Microwave synthesis, single crystal growth and characterization of ZnTe", *Journal of Crystal Growth*, 186 (1998) 535-542.

[10] L. Li, Y. Yang, X. Huang, G. Li and L. Zhang, "Fabrication and Characterization of Single-Crystalline ZnTe Nanowire Arrays", *Journal of Physical Chemistry B*, 109 (2005) 12394-12398.

[11] M. S. Hossain, R. Islam, M. Shahjahan and K. A. Khan, "Studies on the thermoelectric effect in semiconducting ZnTe thin films", *J. Mater. Sci.: Mater. Electron.*, 19 (2008) 1114–1121.

[12] S. V. Ovsyannikov and V. V. Shchennikov, "Thermoelectric properties of the trigonal and orthorhombic modifications of Zinc Telluride", *JETP Letters*, 80 (2004) 35–38.

[13] A. A. Ebnalwaled, "On the conduction mechanism of p-type GaSb bulk crystal", *Mater. Sci. Eng. B*, 174 (2010) 285-289.

[14] A. A. Ebnalwaled, "Evolution of growth and enhancement in power factor of InSb bulk crystal", *J. Cryt. Growth.*, 311 (2009) 4385-4390.

[15] X. L. Su, H. Li and X. F. Tang, "Synthesis and thermoelectric properties of p-type Zn-doped $Zn_xIn_{1-x}Sb$ compounds", *J.Phys. D: Appl. Phys.*43 (2010) 015403-6.

[16] Y. Pei and D. T. Morelli, "Vacancy phonon scattering in thermoelectric In_2Te_3–InSb solid solutions", *Appl. Phys. Lett.* 94 (2009) 122112.

[17] C. H. Jan and Y. A. Chang, "The existence of Ni_3MSb phases in ternary nickel-M-antimony systems (where "M" represents aluminum, gallium, or indium)", *J. Mater. Res.*, 6 (1991) 2660-2665.

[18] T. Sands, V. G. Keramidas, J. Washburn, and R. Gronsky, "Structure and composition of Ni_xGaAs", *Appl. Phys. Lett.* 48 (1986) 402-404.

[19] S. Banerjee, A. Dan and D. Chakravorty, "Review Synthesis of Conducting Nanowires", *Journal of Materials Science*, 37 (2002) 4261-4271.

[20] W. K. Liu, E. G. Karpov and H. S. Park, *Nano Mechanics and Materials*, John Wiley & Sons, Inc., England (2006).

[21] V. S. Panov, "Nanotechnoloies in Production of Solid Alloys (Review)", *Russian Journal of Non-Ferrous Metals*, 48 (2007) 148-152.

[22] C. Mastrovito, J. W. Lekse and J. A. Aitken, "Rapid solid-state synthesis of binary group 15 chalcogenides using microwave irradiation", *Journal of Solid State Chemistry*, 180 (2007) 3262-3270.

[23] J. W. Lekse, A. M. Pischera and J. A. Aitken, "Understanding solid-state microwave synthesis using the diamond-like semiconductor, $AgInSe_2$, as a case study", *Materials Research Bulletin*, 42 (2007) 395-403.

[24] K. Koumoto, I. Terasaki and R. Funahashi, "Complex oxide materials for potential thermoelectric applications", *Mater. Res. Soc. Bull.*, 31 (2006) 206–210.

[25] G. J. Snyder, T. Caillat and J. P. Fleurial, "Thermoelectric transport and magnetic properties of the polaron semiconductor $Fe_xCr_{3-x}Se_4$", *Phys. Rev. B*, 62 (2000) 10185-10193.

[26] G. A. Slack, *Solid State Physics*, Academic Press, New York (1979).

[27] L. D. Hicks and M. S. Dresselhaus, "Effect of quantum-well structures on the thermoelectric figure of merit", *Phys. Rev. B*, 47 (1993) 12727–12731.

[28] J. M. O. Zide, D. Vashaee, Z. X. Bian, G. Zeng, J. E. Bowers, A. Shakouri, and A. C. Gossard, "Demonstration of electron filtering to increase the Seebeck coefficient in $In_{0.53}Ga_{0.47}As/In_{0.53}Ga_{0.28}Al_{0.19}As$ superlattices", *Phys. Rev. B*, 74 (2006) 205335.

[29] Wikipedia. 2009. "Dielectric heating". [Online]. Available: http://en.wikipedia.org/wiki/Dielectric_heating (2009, August 31).

[30] K. J. Rao, B. Vaidhyanathan, M. Ganguli and P. A. Tamakrishnan, "Synthesis of Inorganic Solids Using Microwaves", *Chemistry of Materials*, 11 (1999) 882-895.

[31] J. D. Houmes and H. C. zur Loye, "Plasma Nitridation of metal oxide", *Chemistry of Materials*, 8 (1996) 2551.

[32] J. D. Houmes and H. C. zur Loye, "Microwave Synthesis of Ternary Nitride Materials", *Journal of Solid State Chemistry*, 130 (1997) 266-271.

[33] R. E. Douthwaite, M. L. H. Green and M. Rosseinsky, "Synthesis, reactivity, structure and electronic properties of $[N(CH_3)_4]C_{60}\cdot 1.5$thf: Fullerides with simple hexagonal packing", *Chemistry of Materials*, 8 (1996) 1913-1920.

[34] S. C. Cho, H. S. Uhm, Y. C. Hong and J. H. Kim, "Properties of microwave plasma torch operating at a low pressure", *Physics of Plasma*, 15 (2008) 103503-8.

[35] Y. C. Hong, C. U. Bang, D. H. Shin and H. S. Uhm, "Band gap narrowing of TiO_2 by nitrogen doping in atmospheric microwave plasma", *Chemical Physics Letters*, 413 (2005) 454-457.

[36] R. E. Douthwaite, M. L. H. Green and M. J. Rosseinsky, "Rapid Synthesis of Alkali-Metal Fullerides Using a Microwave-Induced Argon Plasma", *Chemistry of Materials*, 8 (1996) 394-400.

[37] C. F. Wu, R. J. Zhan, X. D. Zhu, W. Huang and C. Wang, "A homogeneous microwave plasma and its application in material surface modification", *Surface and Coating Technology*, 131 (2000) 26-28.

[38] D. H. Shin, C. U. Bang, J. H. Kim, K. H. Han, Y. C. Hong, H. S. Uhm, D. K. Park and K. H. Kim, "Modification of metal surface by microwave plasma at atmospheric pressure", *Surface and Coating Technology*, 201 (2007) 4939-4942.

[39] Y. C. Hong and H. S. Uhm, "Synthesis of MgO nanopowder in atmospheric microwave plasma torch", *Chemical Physics Letters*, 422 (2006) 174-178.

[40] Q. Zhen, G. M. Kale, W. He and J. Liu, "Microwave Plasma Sintered Nanocrystalline BiO-HfO-YO Composite Solid Electrolyte", *Chemistry of Materials*, 19 (2007) 203-210.

[41] J. W. Lekse, T. J. Stagger and J. A. Aitken, "Microwave Metallurgy: Synthesis of Intermetallic Compounds via Microwave Irradiation", *Chemistry of Materials*, 19 (2007) 3601-3603.

[42] U. Schubert and N. Husing, "Synthesis of Inorganic Materials" Wiley-vch press, Germany (2000).

[43] D. W. Rowe, "Thermoelectrics Handbook Macro to Nano" CRD Press, Boca Raton (2006).

[44] Wikipedia. 2011. "Sintering". [Online]. Available: http://en.wikipedia.org/wiki/Sintering (2011, February 01).

[45] Wikipedia. 2009. "Zinc telluride". [Online]. Available: http://en.wikipedia.org/wiki/Zinc_Telluride (2009, September 2).

[46] Wikipedia. 2009. "Zinc telluride". [Online]. Available: http://www.issp.ac.ru/lpcbc/DANDP/znte_adv.html (2009, September 2).

[47] Wikipedia. 2009. "Wurzite". [Online]. Available: http://en.wikipedia.org/wiki/Wurzite (2009, September 2).

[48] S. H. Lee, Y. J. Kim and J. Park, "Shape Evolution of ZnTe Nanocrystals: Nanoflowers, Nanodots, and Nanorods", *Chemistry of Materials*, 19 (2007) 4670-4675.

[49] D. D. Fanfair and B. A. Korgel, "ZnE (E=S, Se, Te) Nanowires Grown by the Solution#Liquid#Solid Mechanism: Importance of Reactant Decomposition Kinetics and the Solvent", *Crystal Growth & Design*, 8 (2008) 3246-4252.

[50] Y. Z. Huang, L. Chen and L. M. Wu, "Submicrosized Rods, Cables, and Tubes of ZnTe (E = S, Se, Te): Exterior#Interior Boron-Chalcogen Conversions and Optical Properties", *Inorganic Chemistry*, 47 (2008) 10723-10728.

[51] Q. Meng, C. Jiang and S. X. Mao, "Temperature-dependent growth of zinc-blende-structured ZnTe nanostructures", *Journal of Crystal Growth*, 310 (2008) 4481-4486.

[52] Y. Guo, B. Geng, L. Zhang, F. Zhan and J. You, "Fabrication, characterization, and strong exciton emission of multilayer ZnTe nanowire superstructures", *The Journal of Physical Chemistry C*, 112 (2008) 20307-20311.

[53] T. Tanaka, K. Hayashida, S. Wang, Q. Guo, M. Nishio and H. Ogawa, " Growth and optical properties of high-quality ZnTe homoepitaxial layers by metalorganic vapor phase epitaxy", *Journal of Crystal Growth*, 248 (2003) 43-49.

[54] Y. Kume, Q. Guo, T. Takaka, M. Nishio, H. Ogawa and W. Shen, "Low-pressure metalorganic vapor epitaxy growth of ZnTe", *Journal of Crystal Growth,* 298 (2007) 441-444.

[55] M. Nishio, K. Hayashida, Q. Gao and H. Ogawa, "Growth rate characteristics and photoluminescence properties of ZnTe in MOVPE system", *Applied Surface Science*, 169-170 (2001) 227-230.

[56] J. Zhang, K. Sun, A. Kumbhar and J. Fang, "Shape-Control of ZnTe Nanocrystal Growth in Organic Solution", *The Journal of Physics Chemistry C*, 112 (2008) 5454-5458.

[57] T. L. Anderson, H. B. Krause, "Refinement of the Sb_2Te_3 and Sb_2Te_2Se structures and their relationship to nonstoichiometric $Sb_2Te_{3-y}Se_y$ compounds" *Acta Crystallogr.* B 30 (1973) 1307-1310.

[58] Q. L. Yuan, Q. L. Nie and D. X. Hau, "Preparation and characterization of the antimony telluride hexagonal nanoplate", *Current Applied Physics*, 9 (2009) 224–226.

[59] W. Wang, B. Poudel, J. Yang, D. Z. Wang and Z. F. Ren, "High-yield synthesis of single-crystalline antimony telluride hexagonal nanoplate using sa solvothermal approach", *J. Am. Chem. Soc.*, 127 (2005) 13792-13793.

[60] B. Zhou, Y. Ji, Y. F. Yang, X. H. Li and J. J. Zhu, "Rapid microwave-assisted synthesis of single-crystalline Sb_2Te_3 hexagonal nanoparticles", *Cryst. Growth Des.*, 8 (2008) 4394-4397.

[61] W. Shi, J. Yu, H. Wang and H. Zhang, "Hydrothermal Synthesis of Single-Crystalline Antimony Telluride Nanobelts", *J. Am. Chem. Soc.*, 128 (2006) 16490-16491.

[62] B. Zhang, Z. Xiao, B. Chhay, R. L. Zimmerman, M. E. Edwards and D. Ila, "Thermoelectric properties of MeV Si ion bombarded Bi_2Te_3/Sb_2Te_3 superlattice deposited by magnetron sputtering", *Surface & Coatings Technology*, 203 (2009) 2682-2686.

[63] S. S. Garje, D. J. Eisler, J. S. Ritch, M. Afzaal, P. O'Brien and T. Chivers, "A New Route to Antimony Telluride Nanoplates from a Single-Source Precursor", *J. Am. Chem. Soc.*, 128 (2006) 3120-3121.

[64] C. Jin, G. Zhang, T. Qian, X. Li and Z. Yao, "Large-Area Sb_2Te_3 Nanowire Arrays", *J. Phys. Chem. B*, 109 (2005) 1430-1432.

[65] R. S. Rawat, P. Arun, A. G. Vedeshwar, Y. L. Lam, M. H. Liu, P. Lee, S. Lee and A. C. H. Huan, "Effect of argon ion irradiation on Sb_2Te_3 films in a dense plasma focus device", *Materials Research Bulletin*, 35 (2000) 477-486.

[66] P. Arun and A. G. Vedeshwar, " Influence of grain size on the electrical properties of Sb_2Te_3 polycrystalline films", *Materials Research Bulletin*, 38 (2003) 1929-1938.

[67] J. S. Lee, S. Brittman, D. Yu and H. Park, "Vapor–Liquid–Solid and Vapor–Solid Growth of Phase-Change Sb_2Te_3 Nanowires and Sb_2Te_3/GeTe Nanowire Heterostructures", *J. Am. Chem. Soc.*, 130 (2008) 6252-6258.

[68] C. H. Jan and Y. A. Chang, "The existence of Ni_3MSb phases in ternary nickel-M-antimony systems (where "M" represents aluminum, gallium, or indium)", *J. Mater. Res.*, 6 (1991) 2660-2665.

[69] S. Tsunekawa, T. Fukuda, and A. Kasuya, "Blue shift in ultraviolet absorption spectra of monodisperse CeO_{2-x} nanoparticles", *J. Appl. Phys.* 87 (2000) 1318-1321.

[70] Powder Diffract. File, JCPDS-ICDD, 12 Campus Boulevard, Newtown Square, PA 19073-3273, U.S.A. (2001).

[71] C. Suryanarayana, M. G. Norton, *X-ray Diffract.*, A Pract. Appro., Plenum Press, New York (1998).

[72] O. Levenspiel, *Chemical Reaction Engineering*, 3 rd ed., John Wiley & Sons, Inc., United states of America (1999).

[73] C. Boudias, D. Monceau, CaRIne Crystallography 3.1, DIVERGENT S.A., Centre de Transfert, 60200 Compiègne, France (1989-1998).

[74] L. Yang, Q. Shen, J. Zhou and K. Jiang, "Biomimetic synthesis of CdS nanocrystals in aqueous solution of pepsin", *Materials Chemistry and Physics*, 98 (2006) 125–130.

[75] K. W. Andrews, D. J. Dyson, S. R. Keown, *Interpret. Electr. Diffract. Patterns*, Plenum Press, New York (1971).

[76] K. T. Yong, Y. Sahoo, H. Zeng, M. T. Swihart, J. R. Minter and P. N. Prasad, "Formation of ZnTe Nanowires by Oriented Attachment", *Chemistry of Materials*, 19 (2007) 4108-4110.

[77] Y. M. Zuev, J. S. Lee, C. Galloy, H. Park and P. Kim, "Diameter Dependence of the Transport Properties of Antimony Telluride Nanowires", *Nano Lett.* 10 (2010) 3037-3040.

[78] G. Y. Chen, W. X. Zhang, and A. W. Xu, "Synthesis and characterization of single-crystal Sb_2S_3 nanotubes via an EDTA-assisted hydrothermal route", *Materials Chemistry and Physics*, 123 (2010) 236-240.

[79] Q. A. Zhu, M. Gong, C. Zhang, G. Yong, S. Xiang, "Preparation of Sb_2S_3 nanomaterials with different morphologies via a refluxing approach", *J. Cryst. Growth*, 311 (2009) 3651-3655.

[80] İ. Y. Erdoğan, Ü. Demir, "Synthesis and characterization of Sb_2Te_3 nanofilms via electrochemical co-deposition method", Journal of Electroanalytical Chemistry, 633 (2009) 253-258.

[81] J. Yang, W. Zhu, X. Gao, S. Bao, X. Fan, X. Duan, J. Hou, "Formation and Characterization of Sb_2Te_3 Nanofilms on Pt by Electrochemical Atomic Layer Epitaxy", *J. Phys. Chem. B*, 110 (2006) 4599-4604.

[82] F. Izumi and K. Momma, "Three-dimensional visualization in powder diffraction", *Solid State Phenomomena*, 130 (2007) 15-20.

[83] T. Sands, V. G. Keramidas, J. Washburn, and R. Gronsky, "Structure and composition of Ni_xGaAs", *Appl. Phys. Lett.*, 48 (1986) 402-404.

[84] A. A. Ebnalwaled, "On the conduction mechanism of p-type GaSb bulk crystal", *Mater. Sci. Eng. B*, 174 (2010) 285-289.

[85] J. H. Seol, A. L. Moore, S. K. Saha, F. Zhou, L. Shi, Q. L. Ye, R. Scheffler, N. Mingo and T. Yamada, "Measurement and analysis of thermopower and electrical conductivity of an indium antimonide nanowire from a vapor-liquid-solid method" *J. Appl. Phys.*, 101 (2007) 023706-6.

APPENDICES

APPENDIX A

The Joint Committee for Powder Diffraction Standards (JCPDS) [78]

1. ZnTe, JCPDS file number 15-0746

Name and formula

Reference code:	15-0746	Empirical formula:	TeZn
PDF index name:	Zinc Telluride	Chemical formula:	ZnTe

Crystallographic parameters

Crystal system:	Cubic	Alpha (degree):	90.0000
Space group:	F-43m	Beta (degree):	90.0000
Space group number:	216	Gamma (degree):	90.0000
a (Å):	6.1026	Calculated density:	5.37
b (Å):	6.1026	Volume of cell:	227.27
c (Å):	6.1026	Z:	4.00
		RIR:	9.30

Subfiles and Quality

Subfiles:	Inorganic Alloy, metal or intermetalic Common Phase
	Educational pattern, NBS pattern
Quality:	Star (S)

Comments

Color:	Reddish brown
Sample source:	Sample was obtained from Semi-Elements, Inc.,
	Saxonburg, Pennsylvania, USA.

Analysis: Spectrographic analysis: 0.01-0.1% of Si; 0.001-0.01% each of Al, Ba, Fe, and Mg.

Temperature: Pattern taken at 25 C.

References

Primary reference: *Natl. Bur. Stand. (U.S.) Monogr. 25*, **3**, 58, (1964)

Peak list

No.	h	k	l	d [A]	I [%]	No.	h	k	l	d [A]	I [%]
1	1	1	1	3.52300	100.0	11	4	4	0	1.07890	4.0
2	2	0	0	3.05100	10.0	12	5	3	1	1.03150	6.0
3	2	2	0	2.15900	80.0	13	6	0	0	1.01710	2.0
4	3	1	1	1.84000	35.0	14	6	2	0	0.96480	6.0
5	2	2	2	1.76200	4.0	15	5	3	3	0.93070	4.0
6	4	0	0	1.52600	8.0	16	6	2	2	0.92000	2.0
7	3	3	1	1.40030	14.0	17	4	4	4	0.88080	2.0
8	4	2	0	1.36450	4.0	18	5	5	1	0.85450	6.0
9	4	2	2	1.24560	10.0	19	6	4	2	0.81550	8.0
10	5	1	1	1.17450	8.0	20	7	3	1	0.79450	6.0

Stick Pattern

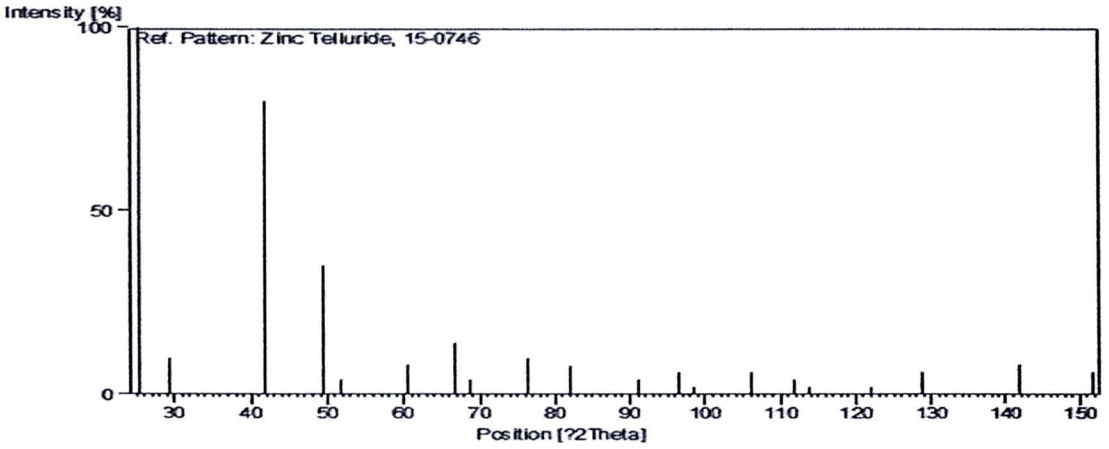

2. Zn, JCPDS file number 01-1238

Name and formula

Reference code:	01-1238	Empirical formula:	Zn
PDF index name:	Zinc	Chemical formula:	Zn

Crystallographic parameters

Crystal system:	Hexagonal	Alpha (degree):	90.0000
Space group:	P63/mmc	Beta (degree):	90.0000
Space group number:	194	Gamma (degree):	120.0000
a (Å):	2.6591	Measured density:	7.10
b (Å):	2.6591	Volume of cell:	30.22
c (Å):	4.9353	Z:	2.00
		RIR:	-

Status, subfiles and quality

Status:	Marked as deleted by ICDD
Subfiles:	Inorganic
Quality:	Blank (B)

Comments

Deleted by:	Deleted by NBS card.
Color:	White
Melting point:	420

References

Primary reference:	Hanawalt et al., *Anal. Chem.*, **10**, 475, (1938)
Unit cell:	*Dana's System of Mineralogy, 7th Ed.*

Peak list

No.	h	k	l	d [A]	I [%]	No.	h	k	l	d [A]	I [%]
1	0	0	2	2.46000	25.0	6	1	1	2	1.17000	12.0
2	1	0	0	2.30000	20.0	7	2	0	1	1.12000	8.0
3	1	0	1	2.08000	100.0	8	2	0	2	1.04000	2.0
4	1	0	2	1.68000	14.0	9	2	0	3	0.94000	2.0
5	1	1	0	1.33000	18.0	10	1	0	5	0.91000	2.0

Stick Pattern

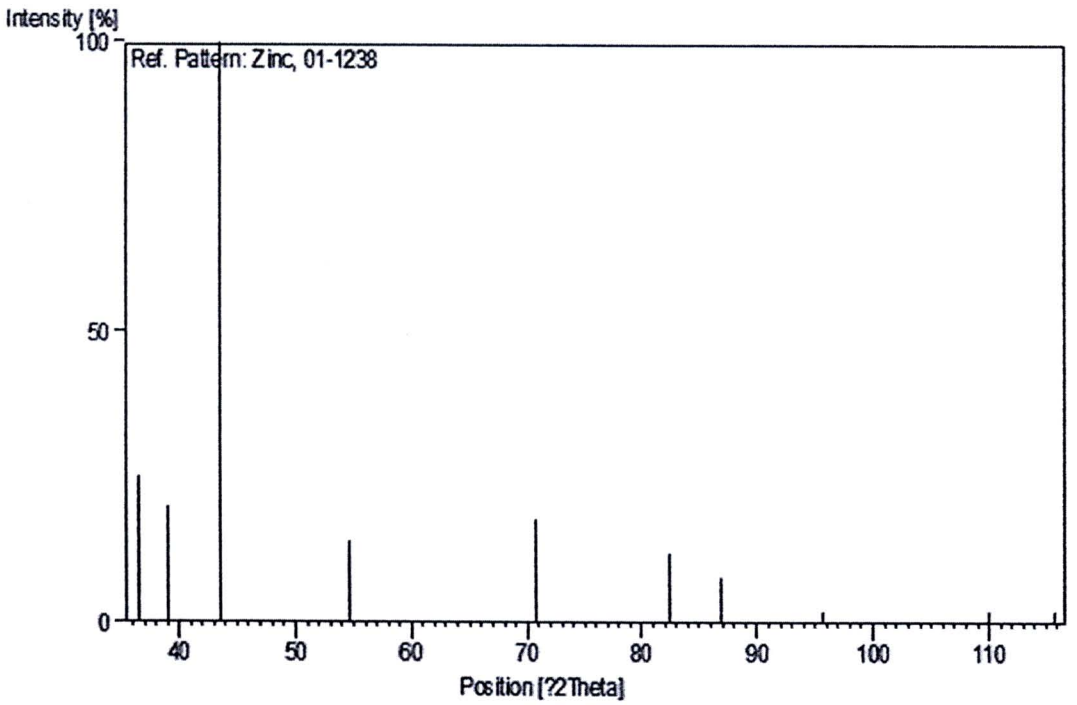

3. Te, JCPDS file number 01-0714

Name and formula

Reference code:	01-0714	Empirical formula:	Te
PDF index name:	Tellurium	Chemical formula:	Te

Crystallographic parameters

Crystal system:	Hexagonal	Alpha (degree):	90.0000
Space group:	P312	Beta (degree):	90.0000
Space group number:	149	Gamma (degree):	120.0000
a (Å):	4.4450	Measured density:	6.20
b (Å):	4.4450	Volume of cell:	101.13
c (Å):	5.9100	Z:	3.00
		RIR:	-

Status, subfiles and quality

Status:	Marked as deleted by ICDD
Subfiles:	Inorganic
Quality:	Blank (B)

Comments

Color:	Silvery
Optical data:	B=2.68, Q=3.07, Sign=+
Melting point:	449.8

References

Primary reference:	Hanawalt. et al., *Anal. Chem.*, **10**, 475, (1938)
Unit cell:	*Dana's System of Mineralogy, 7th Ed.*

Peak list

No.	h	k	l	d [A]	I [%]
1	0	0	1	5.80000	19.0
2	1	0	0	3.86000	14.0
3	1	0	1	3.24000	100.0
4	1	0	2	2.34000	48.0
5	1	1	0	2.22000	32.0
6	1	1	1	2.08000	14.0
7	0	0	3	1.96000	14.0
8	2	0	1	1.83000	28.0
9	1	1	2	1.77000	10.0
10	2	0	2	1.61000	20.0
11	1	1	3	1.47000	28.0
12	2	1	1	1.42000	13.0
13	1	0	4	1.38000	16.0
14	2	1	2	1.31000	8.0
15	3	0	1	1.26000	5.0
16	0	0	5	1.18000	14.0
17	2	2	0	1.12000	5.0
18	3	1	1	1.05000	5.0
19	2	0	5	1.01000	5.0
20	3	0	4	0.97000	2.0
21	3	0	5	0.87000	2.0

Stick Pattern

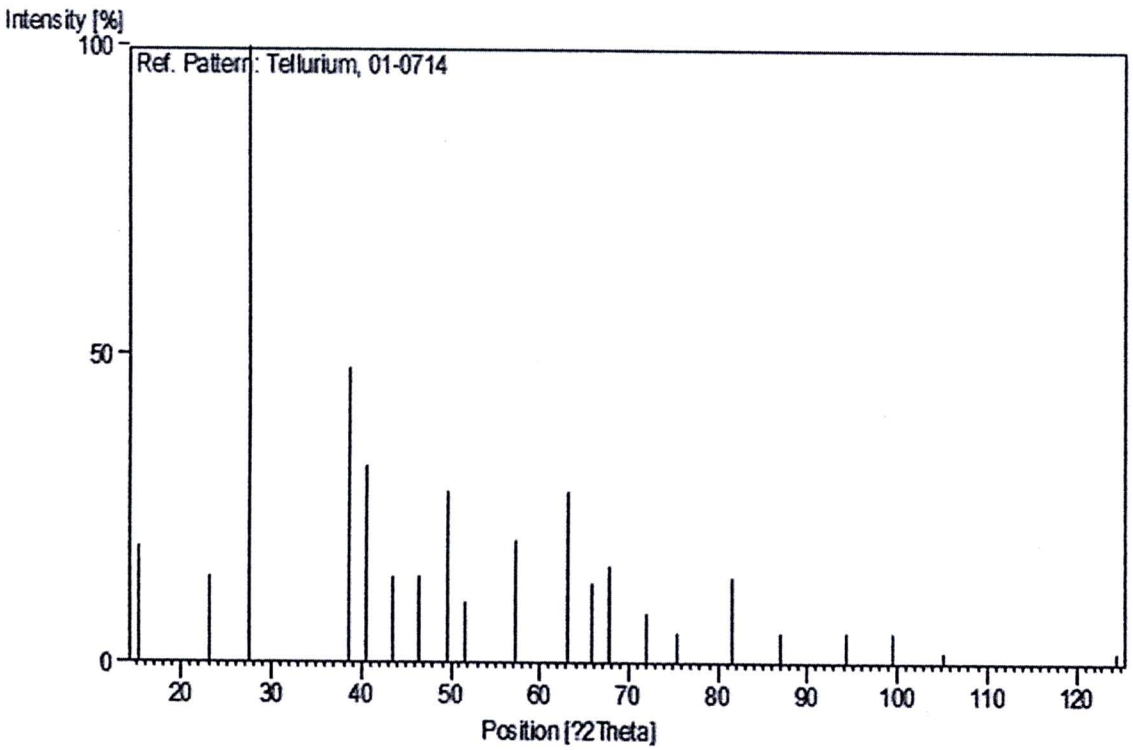

4. Te, JCPDS file number 36-1452

Name and formula

Reference code:	36-1452	Empirical formula:	Te
PDF index name:	Telluride	Chemical formula:	Te

Crystallographic parameters

Crystal system:	Hexagonal	Alpha (degree):	90.0000
Space group:	P3121	Beta (degree):	90.0000
Space group number:	152	Gamma (degree):	120.0000
a (Å):	4.4579	Calculated density:	6.23
b (Å):	4.4579	Volume of cell:	102.01
c (Å):	5.9270	Z:	3.00
		RIR:	-

Status, subfiles and quality

Status:	-
Subfiles:	Inorganic, Mineral, Alloy, Metal or Intermetalic, Common Phase, Educational pattern, Forensic, NBS pattern
Quality:	Star (S)

Comments

Color:	Gray metallic
General comments:	The structure was determined by Bradley (1). Hexagonal close packed.

Color values in air C illuminant: x .311 .308, y .318 .317, Y% 59.9 69.4, ld 560 495, Pe% 0.7 0.6.

QDF-2.

On synthetic material.

Sample source: The sample was from the Fisher Scientific Co., Fair Lawn, NJ, USA. It was ground and annealed at 300 C for 1/2 hour.

Polymorphism: There are several high pressure polymorphs of tellurium.

Additional pattern: To replace 4-554 (2).

Temperature: The mean temperature of data collection was 25.41 °C.

References

Primary reference: McMurdie, H., Morris, M., Evans, E., Paretzkin, B., Wong-Ng, W., Ettlinger, L., Hubbard, C., Powder Diffraction, 1, 76, (1986)

Structure: 1. Bradley, A., Philos. Mag., 48, 477, (1924)

Additional pattern: 2. Swanson, H., Tatge, E., Natl. Bur. Stand. (U.S.), Circ. 539, 1, 26, (1953)

Peak list

No.	h	k	l	d [A]	I [%]	No.	h	k	l	d [A]	I [%]
1	1	0	0	3.85643	16.0	5	1	1	1	2.08643	8.0
2	1	0	1	3.23356	100.0	6	0	0	3	1.97545	9.0
3	1	0	2	2.35047	36.0	7	2	0	0	1.93001	3.0
4	1	1	0	2.22839	25.0	8	2	0	1	1.83540	14.0

No.	h	k	l	d [A]	I [%]	No.	h	k	l	d [A]	I [%]
9	1	1	2	1.78135	4.0	22	2	0	4	1.17513	4.0
10	1	0	3	1.75904	2.0	23	2	1	3	1.17387	3.0
11	2	0	2	1.61752	8.0	24	1	0	5	1.13299	1.0
12	1	1	3	1.47824	7.0	25	2	2	0	1.11467	1.0
13	2	1	0	1.45865	5.0	26	2	2	1	1.09532	1.0
14	2	1	1	1.41652	4.0	27	3	0	3	1.07832	1.0
15	1	0	4	1.38363	4.0	28	3	1	0	1.07084	1.0
16	2	0	3	1.38110	4.0	29	3	1	1	1.05346	1.0
17	2	1	2	1.30906	3.0	30	1	1	5	1.04680	1.0
18	3	0	0	1.28698	1.0	31	2	2	2	1.04337	1.0
19	3	0	1	1.25767	2.0	32	2	1	4	1.03962	1.0
20	1	1	4	1.23411	1.0	33	2	0	5	1.01005	1.0
21	3	0	2	1.18030	1.0	34	3	1	2	1.00708	1.0

Stick Pattern

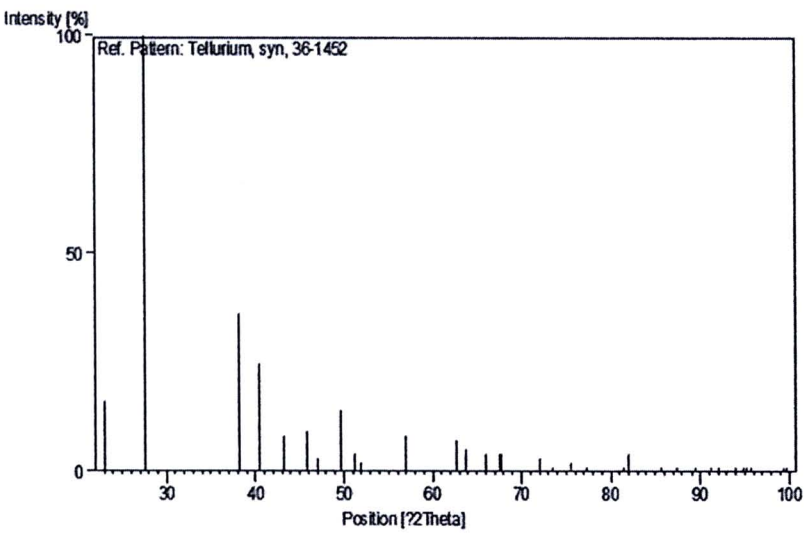

5. Sb_2Te_3, JCPDS file number 15-0874

Name and formula

Reference code:	15-0874	Empirical formula:	Sb_2Te_3
PDF index name:	Antimony Telluride	Chemical formula:	Sb_2Te_3

Crystallographic parameters

Crystal system:	Rhombohedral	Alpha (degree):	90.0000
Space group:	R-3M	Beta (degree):	90.0000
Space group number:	166	Gamma (degree):	120.0000
a (Å):	4.2620	Calculated density:	6.51
b (Å):	4.2620	Volume of cell:	479.01
c (Å):	30.4500	Z:	3.00
		RIR:	-

Status, subfiles and quality

Status:	-
Subfiles:	Inorganic, Mineral, Alloy, Metal or Intermetalic
Quality:	Indexed (I)

Comments

Color:	Dark gray
General comments:	Mineral occurs at Mattagami Lake mine, Galinee Twp., Quebec, Canada, Thorpe, R. et al., Can. Mineral., 12 55 (1973).
Sample source:	Sample was obtained from Semitronics, Inc., Winchester, Massachusetts, USA.

Sample preparation: The sample was heated overnight in an evacuated tube.

Analysis: Spectroscopic analysis: 0.001 to 0.01% each of Al and Si.

Unit cell: Rhombohedral cell: a=10.444, a=23.55.

Temperature: Pattern taken at 25 °C.

References

Primary reference: Natl. Bur. Stand. (U.S.) Monogr. 25, 3, 8, (1964)

Unit cell: Am. Mineral., 59, 383, (1974)

Peak list

No.	h	k	l	d [A]	I [%]	No.	h	k	l	d [A]	I [%]
1	0	0	3	10.16000	2.0	15	1	1	9	1.80400	2.0
2	0	0	6	5.08000	4.0	16	2	0	5	1.76600	10.0
3	0	0	9	3.38300	6.0	17	0	0	18	1.69200	2.0
4	1	0	4	3.32100	2.0	18	2	0	8	1.66100	1.0
5	0	1	5	3.15700	100.0	19	0	1	17	1.61100	2.0
6	1	0	7	2.81500	1.0	20	0	2	10	1.57800	8.0
7	0	1	8	2.65100	2.0	21	2	0	11	1.53700	2.0
8	1	0	10	2.34900	35.0	22	1	0	19	1.47000	8.0
9	0	1	11	2.21500	6.0	23	0	0	21	1.45000	2.0
10	1	1	0	2.13000	25.0	24	0	1	20	1.40800	2.0
11	0	0	15	2.03000	4.0	25	1	2	5	1.35970	8.0
12	1	0	13	1.97700	4.0	26	0	2	16	1.32490	2.0
13	1	1	6	1.96400	2.0	27	2	1	10	1.26830	6.0
14	0	1	14	1.87500	4.0	28	0	1	23	1.24620	2.0

No.	h	k	l	d [A]	I [%]
29	3	0	0	1.23030	2.0
30	0	2	19	1.21020	2.0
31	1	1	21	1.19880	1.0
32	1	2	14	1.17420	2.0
33	3	0	9	1.15630	1.0
34	2	1	16	1.12520	1.0
35	2	0	23	1.07590	1.0
36	2	2	0	1.06550	2.0
37	3	0	15	1.05220	1.0
38	1	0	28	1.04310	1.0
39	1	2	20	1.02860	1.0
40	0	2	25	1.01670	1.0
41	0	1	29	1.00960	1.0
42	3	0	18	0.99520	1.0
43	1	3	10	0.97040	1.0
44	2	2	15	0.94340	1.0

Stick Pattern

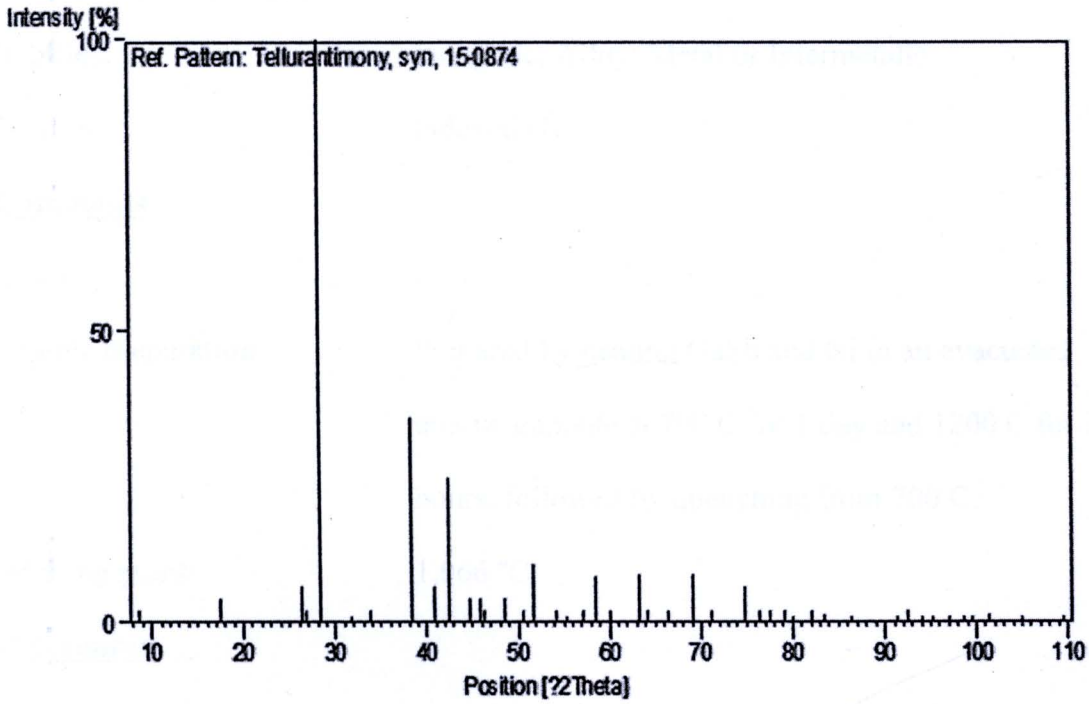

6. Ni_3GaSb, JCPDS file number 47-1401

Name and formula

Reference code:	47-1401	Empirical formula:	Ni_3GaSb
PDF index name:		Chemical formula:	Ni_3GaSb
	Antimony Gallium Nickel		

Crystallographic parameters

Crystal system:	Hexagonal	Alpha (degree):	90.0000
Space group:	P63/mmc	Beta (degree):	90.0000
Space group number:	194	Gamma (degree):	120.0000
a (Å):	4.0000	Measured density:	-
b (Å):	4.0000	Volume of cell:	70.53
c (Å):	5.0900	Z:	1.00
		RIR:	-

Status, subfiles and quality

Subfiles:	Inorganic, Alloy, Metal or Intermetalic
Quality:	Indexed (I)

Comments

Color:	-
Sample preparation:	Prepared by heating GaSb and Ni in an evacuated quartz ampoule at 700 C for 1 day and 1200 C for 2 hours, followed by quenching from 700 C.
Melting point:	1,066 °C

References

Primary reference: Jan, C.-H., Chang, Y., *J. Mater. Res.*, **6**, 2660, (1991)

Peak list

No.	h	k	l	d [A]	I [%]	No.	h	k	l	d [A]	I [%]
1	1	0	1	2.86600	76.0	7	1	0	3	1.52300	12.0
2	0	0	2	2.54800	12.0	8	2	0	2	1.43100	28.0
3	1	0	2	2.05200	100.0	9	0	0	4	1.26900	9.0
4	1	1	0	2.00000	84.0	10	-	-	-	1.25400	2.0
5	2	0	1	1.63900	14.0	11	2	1	2	1.16300	18.0
6	1	1	2	1.57200	13.0	12	3	0	0	1.15400	7.0

Stick Pattern

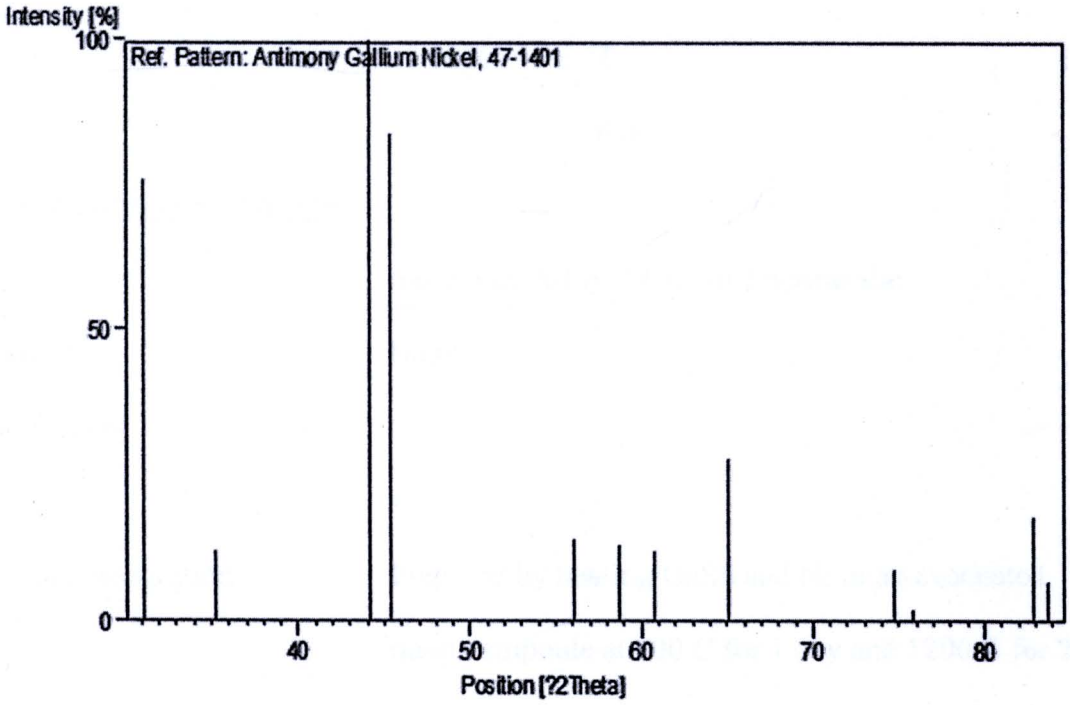

7. Ni_3InSb, JCPDS file number 47-1402

Name and formula

Reference code:	47-1402	Empirical formula:	Ni_3InSb
PDF index name:		Chemical formula:	Ni_3InSb
Antimony Indium Nickel			

Crystallographic parameters

Crystal system:	Hexagonal	Alpha (degree):	90.0000
Space group:	P63/mmc	Beta (degree):	90.0000
Space group number:	194	Gamma (degree):	120.0000
a (Å):	4.0000	Measured density:	-
b (Å):	4.0000	Volume of cell:	75.92
c (Å):	5.0900	Z:	1.00
		RIR:	-

Status, subfiles and quality

Subfiles:	Inorganic, Alloy, Metal or Intermetalic
Quality:	Blank (B)

Comments

Color:	-
Sample preparation:	Prepared by heating GaSb and Ni in an evacuated quartz ampoule at 700 C for 1 day and 1200 C for 2 hours, followed by quenching from 700 C.
Melting point:	1,091°C

References

Primary reference: Jan, C.-H., Chang, Y., *J. Mater. Res.*, **6**, 2660, (1991)

Peak list

No.	h	k	l	d [A]	I [%]	No.	h	k	l	d [A]	I [%]
1	1	0	1	2.94600	91.0	7	1	0	3	1.55500	13.0
2	0	0	2	2.59800	17.0	8	2	0	2	1.46800	25.0
3	1	0	2	2.09800	91.0	9	0	0	4	1.30200	11.0
4	1	1	0	2.05700	100.0	10	2	1	2	1.19300	17.0
5	2	0	1	1.68500	18.0	11	3	0	0	1.18600	11.0
6	1	1	2	1.61200	16.0						

Stick Pattern

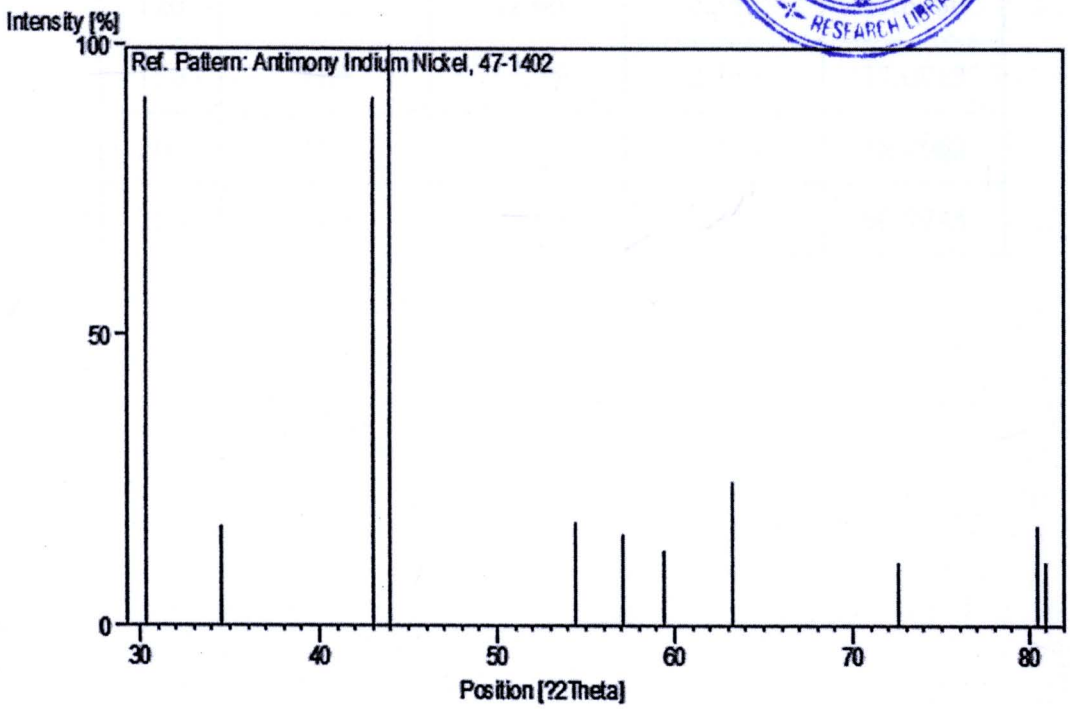

APPENDIX B

Camera constants used for the indexing of SAED pattern

Table B1. TEM constants ($L\lambda$) at 200 kV

L (cm)	D_{111}Au (mm)	r_{111}Au (mm)	D_{111}Auv (A)	$L\lambda$ (mm.A)
40	8.70	4.35	2.355	10.2442
60	13.2	6.60	2.355	15.5430
80	17.2	8.60	2.355	20.2530
100	21.2	10.60	2.355	24.9630
120	25.2	12.60	2.355	29.6730
150	31.5	15.75	2.355	37.0912
200	41.5	20.75	2.355	48.8662
250	51.8	25.90	2.355	60.9945

APPENDIX C

Microwave induced plasma system

Figure C1. Microwave induced plasma system

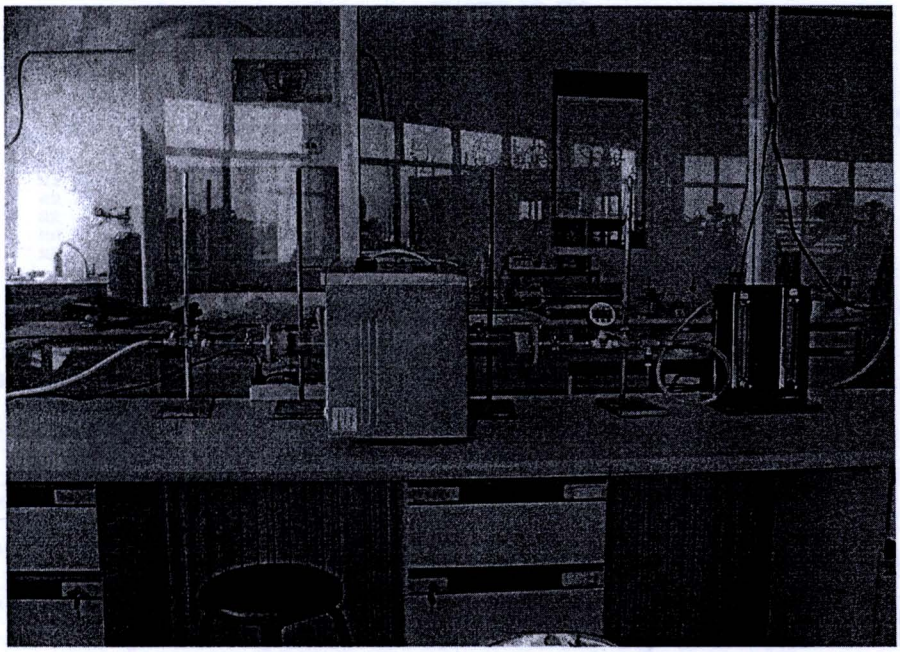

Figure C2. Microwave induced plasma system during operation

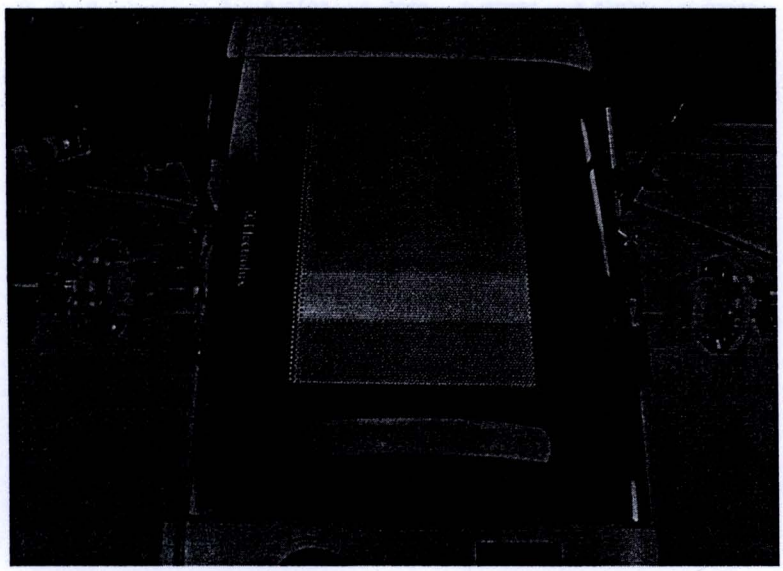

APPENDIX D

The results of the Rietveld refinement analysis

D1. Ni_3GaSb

```
                                                                14:50:37, 2011.02.09
                                  Welcome to the

     RRRRRRRRRRR      IIIIIIII    EEEEEEEEEEE  TTTTTTTTTTT   AAAAAAAAAA     NN          NN
     RRRRRRRRRRRR     IIIIIIII    EEEEEEEEEEE  TTTTTTTTTTT  AAAAAAAAAAAA    NNN         NN
     RR         RR       II      EE                TT      AA          AA    NNNN        NN
     RR         RR       II      EE                TT      AA          AA    NN NN       NN
     RR         RR       II      EE                TT      AA          AA    NN  NN      NN
     RRRRRRRRRRRR        II      EEEEEEEEEE        TT      AAAAAAAAAAAA    NN   NN     NN
     RRRRRRRRRRR         II      EEEEEEEEEE        TT      AAAAAAAAAAAA    NN    NN    NN
     RR    RRR           II      EE                TT      AA          AA    NN     NN NN
     RR     RRR          II      EE                TT      AA          AA    NN      NNNN
     RR      RRR         II      EE                TT      AA          AA    NN       NNN
     RR       RRR    IIIIIIII    EEEEEEEEEEE       TT      AA          AA    NN        NN
     RR        RR    IIIIIIII    EEEEEEEEEEE       TT      AA          AA    NN        NN

          system for pattern-fitting structure refinement with X-ray and neutron diffraction data

 *** Data given by user and system ***

     Title: Ni3GaSb

 Reliability factors, goodness-of-fit indicator, and Durbin-Watson statistic

 Rwp =  9.372    Rp =  7.310    RR = 11.355    Re =  5.335    S = 1.7568    d1 = 0.7009    d2 = 0.2701

 Ni3GaSb
  RB =  2.735    RF =  2.161    E(SCIO) =  2692.07
 Lattice parameters (Angstrom or degree) and unit-cell volume (Angstrom**3) in Ni3GaSb

       a          b          c        alpha       beta       gamma          V
   4.01357    4.01357    5.11362    90.0000    90.0000   120.0000     71.3381
   0.00569          -    0.00525          -          -          -      0.1607

 Structure parameters, g, x, y, z, B/Angstrom**2, and U/Angstrom**2, in Ni3GaSb
                                    100*B/nm**2        100*U/nm**2

  Atom      Site                  neq  *   g   =   n       x         y         z         B         U
  Ni          2a  0  0  0           2    0.5000   1.0000  0.00000   0.00000   0.00000   0.500   0.00633
                                     -       -        -       -         -         -       -         -
  Ni1         2a  0  0  0           2    0.5000   1.0000  0.00000   0.00000   0.50000   0.500   0.00633
                                     -       -        -       -         -         -       -         -
  Ni2         2d  1/3 2/3 3/4       2    0.2500   0.5000  0.33330   0.66670   0.75000   0.500   0.00633
                                     -       -        -       -         -         -       -         -
  Ni3         2d  1/3 2/3 3/4       2    0.2500   0.5000  0.66670   0.33330   0.25000   0.500   0.00633
                                     -       -        -       -         -         -       -         -
  Ga          2c  1/3 2/3 1/4       2    0.5000   1.0000  0.33330   0.66670   0.25000   0.500   0.00633
                                     -       -        -       -         -         -       -         -
  Sb          2c  1/3 2/3 1/4       2    0.5000   1.0000  0.66670   0.33330   0.75000   0.500   0.00633
                                     -       -        -       -         -         -       -         -
```

*** Summary of possible reflections (based on the refined parameters) ***

No.	Phase	h	k	l	Code	2-theta	d	Iobs	Ical	|F(nucl)|	|F(magn)|	POF	FWHM	m	Dd/d
1	1	1	0	0	1	25.608	3.47586	1358	474	4.1036	-	0.999	0.1022	6	0.00785
2	1	1	0	1	1	31.086	2.87464	59573	61326	40.4328	-	1.000	0.1820	12	0.01142
3	1	0	0	2	1	35.068	2.55681	9886	9912	45.2042	-	1.002	0.2156	2	0.01191
4	1	1	0	2	1	43.925	2.05960	94253	93504	72.3755	-	1.001	0.2969	12	0.01285
5	1	1	1	0	1	45.144	2.00679	100000	99783	109.1533	-	0.999	0.3363	6	0.01412
6	1	2	0	0	1	52.620	1.73793	150	133	4.7215	-	0.999	0.4035	6	0.01424
7	1	2	0	1	1	55.825	1.64549	12001	11653	33.2367	-	0.999	0.4143	12	0.01365
8	1	1	1	2	1	58.413	1.57861	13610	13572	37.6269	-	1.000	0.4188	12	0.01307
9	1	1	0	3	1	60.440	1.53042	8942	9201	32.0841	-	1.002	0.4181	12	0.01253
10	1	2	0	2	1	64.813	1.43732	24308	25753	57.7947	-	1.000	0.4729	12	0.01300
11	1	2	1	0	1	71.795	1.31375	161	164	5.1075	-	0.999	0.5769	12	0.01391
12	1	0	0	4	1	74.105	1.27841	6415	6524	80.7818	-	1.002	0.5129	2	0.01186
13	1	2	1	1	1	74.512	1.27243	9699	9814	28.8337	-	0.999	0.5803	24	0.01332
14	1	2	0	3	1	78.542	1.21692	4666	4256	27.9793	-	1.001	0.5733	12	0.01224
15	1	1	0	4	1	79.883	1.19983	161	145	5.2165	-	1.002	0.5636	12	0.01175
16	1	2	1	2	1	82.479	1.16852	25364	23207	47.8825	-	1.000	0.6338	24	0.01262
17	1	3	0	0	1	83.340	1.15862	14703	13513	73.6650	-	0.999	0.6919	6	0.01357
18	1	3	0	1	1	85.952	1.12998	0	0	0.0193	-	0.999	0.6941	12	0.01300
19	1	1	1	4	1	91.192	1.07821	22743	21430	68.3769	-	1.001	0.6726	12	0.01150
20	1	3	0	2	1	93.759	1.05532	4017	3795	29.0608	-	0.999	0.7533	12	0.01231
21	1	2	1	3	1	95.510	1.04055	H	5529	24.8839	-	1.000	0.7458	24	0.01182
22	1	2	0	4	1	96.836	1.02980	H	128	5.3509	-	1.001	0.7335	12	0.01136
23	1	2	2	0	1	100.294	1.00339	H	8786	63.0800	-	0.999	0.8938	6	0.01302

*** End of job ***

CPU time = 0 min 0.37 s

--- RIETAN-FP v1.8 Copyright 2009 by F. Izumi ---

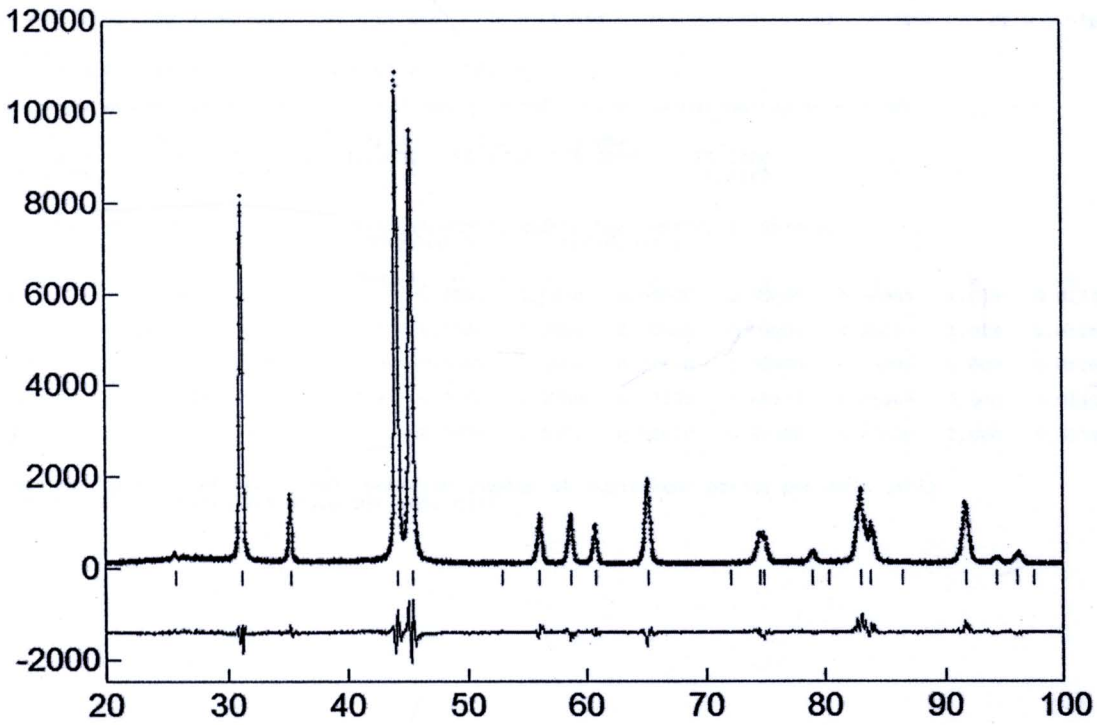

D2. Ni_3InSb

```
                                                                    15:09:42, 2011.02.09
                                    Welcome to the

     RRRRRRRRRR      IIIIIIII    EEEEEEEEEEE  TTTTTTTTTTT   AAAAAAAAAA     NN         NN
     RRRRRRRRRRR     IIIIIIII    EEEEEEEEEEE  TTTTTTTTTTT  AAAAAAAAAAAA    NNN        NN
     RR         RR      II      EE               TT       AA          AA    NNNN       NN
     RR         RR      II      EE               TT       AA          AA    NN NN      NN
     RR         RR      II      EE               TT       AA          AA    NN  NN     NN
     RRRRRRRRRRR        II      EEEEEEEEEE       TT       AAAAAAAAAAAA    NN   NN    NN
     RRRRRRRRRR         II      EEEEEEEEEE       TT       AAAAAAAAAAAA    NN    NN   NN
     RR    RRR          II      EE               TT       AA          AA    NN     NN NN
     RR     RRR         II      EE               TT       AA          AA    NN      NNNN
     RR      RRR        II      EE               TT       AA          AA    NN       NNN
     RR       RRR    IIIIIIII    EEEEEEEEEEE      TT       AA          AA    NN        NN
     RR        RR    IIIIIIII    EEEEEEEEEEE      TT       AA          AA    NN        NN

          system for pattern-fitting structure refinement with X-ray and neutron diffraction data


*** Data given by user and system ***

    Title: Ni3InSb


Reliability factors, goodness-of-fit indicator, and Durbin-Watson statistic

Rwp = 13.677    Rp = 10.206    RR = 16.146    Re =  5.542    S = 2.4679    d1 = 0.5261    d2 = 0.5468

Ni3InSb
 RB =  3.014    RF =  2.793    E(SCIO) =  1785.41

Lattice parameters (Angstrom or degree) and unit-cell volume (Angstrom**3) in Ni3InSb

     a         b         c        alpha      beta      gamma        V
  4.10655   4.10655   5.18241   90.0000   90.0000  120.0000   75.6860
  0.00788         -   0.00722         -         -         -    0.2310

Structure parameters, g, x, y, z, B/Angstrom**2, and U/Angstrom**2, in Ni3InSb
                                    100*B/nm**2          100*U/nm**2

 Atom      Site                    neq  *   g    =   n       x         y         z         B         U
 Ni          2a  0  0  0            2    0.5000    1.0000  0.00000   0.00000   0.00000   1.000     0.01267
                                     -       -         -       -         -         -         -         -
 Ni1         2a  0  0  0            2    0.5000    1.0000  0.00000   0.00000   0.50000   1.000     0.01267
                                     -       -         -       -         -         -         -         -
 Ni2         2d  1/3 2/3 3/4        2    0.5000    1.0000  0.33330   0.66670   0.75000   1.000     0.01267
                                     -       -         -       -         -         -         -         -
 In          2c  1/3 2/3 1/4        2    0.5000    1.0000  0.33330   0.66670   0.25000   2.000     0.02533
                                     -       -         -       -         -         -         -         -
 Sb          2c  1/3 2/3 1/4        2    0.5000    1.0000  0.66670   0.33330   0.75000   2.000     0.02533
                                     -       -         -       -         -         -         -         -

 neq: multiplicity of the Wyckoff position (number of equivalent points per unit cell)
   n: number of equivalent atoms per unit cell
```

*** Summary of possible reflections (based on the refined parameters) ***

No.	Phase	h	k	l	Code	2-theta	d	Iobs	Ical	|F(nucl)|	|F(magn)|	POF	FWHM	m	Dd/d
1	1	1	0	0	1	25.018	3.55637	2919	3201	11.7585	-	0.907	0.1688	6	0.01328
2	1	1	0	1	1	30.460	2.93232	91635	92062	52.4736	-	0.990	0.1861	12	0.01193
3	1	0	0	2	1	34.588	2.59120	17416	17426	57.7384	-	1.217	0.1955	2	0.01096
4	1	1	0	2	1	43.161	2.09427	100000	101161	76.2013	-	1.091	0.2209	12	0.00975
5	1	1	1	0	1	44.068	2.05327	95181	95392	117.5072	-	0.907	0.2382	6	0.01027
6	1	2	0	0	1	51.341	1.77819	652	388	8.8612	-	0.907	0.2718	6	0.00987
7	1	2	0	1	1	54.514	1.68193	14686	13512	38.8872	-	0.933	0.2768	12	0.00938
8	1	1	1	2	1	57.196	1.60928	17569	16385	43.3574	-	1.009	0.2785	12	0.00891
9	1	1	0	3	1	59.436	1.55386	14531	12121	36.4571	-	1.145	0.2774	12	0.00848
10	1	2	0	2	1	63.388	1.46616	23881	23298	58.1702	-	0.990	0.3094	12	0.00875
11	1	2	1	0	1	69.928	1.34418	260	262	7.1101	-	0.907	0.3764	12	0.00939
12	1	2	1	1	1	72.601	1.30113	9615	9210	30.5946	-	0.922	0.3778	24	0.00898
13	1	0	0	4	1	72.961	1.29560	6991	6814	79.5969	-	1.217	0.3338	2	0.00788
14	1	2	0	3	1	76.879	1.23905	4531	4235	28.8970	-	1.047	0.3731	12	0.00820
15	1	1	0	4	1	78.510	1.21734	251	227	6.4301	-	1.172	0.3672	12	0.00784
16	1	2	1	2	1	80.418	1.19319	20141	18395	46.0322	-	0.960	0.4138	24	0.00854
17	1	3	0	0	1	81.051	1.18546	11337	10298	71.3306	-	0.907	0.4546	6	0.00928
18	1	3	0	1	1	83.606	1.15561	0	0	0.0192	-	0.919	0.4556	12	0.00889
19	1	1	1	4	1	89.339	1.09571	20036	18240	63.9591	-	1.112	0.4430	12	0.00782
20	1	3	0	2	1	91.214	1.07800	3231	2881	27.7407	-	0.950	0.4981	12	0.00851
21	1	2	1	3	1	93.122	1.06086	4623	4313	23.4645	-	1.006	0.4939	24	0.00816
22	1	2	0	4	1	94.720	1.04713	126	121	5.3608	-	1.091	0.4871	12	0.00783
23	1	2	2	0	1	97.235	1.02664	H	5814	57.9090	-	0.907	0.5991	6	0.00921
24	1	1	0	5	1	101.448	0.99508	H	2052	21.2330	-	1.186	0.5273	12	0.00753

*** End of job ***

CPU time = 0 min 0.28 s

--- RIETAN-FP v1.8 Copyright 2009 by F. Izumi ---

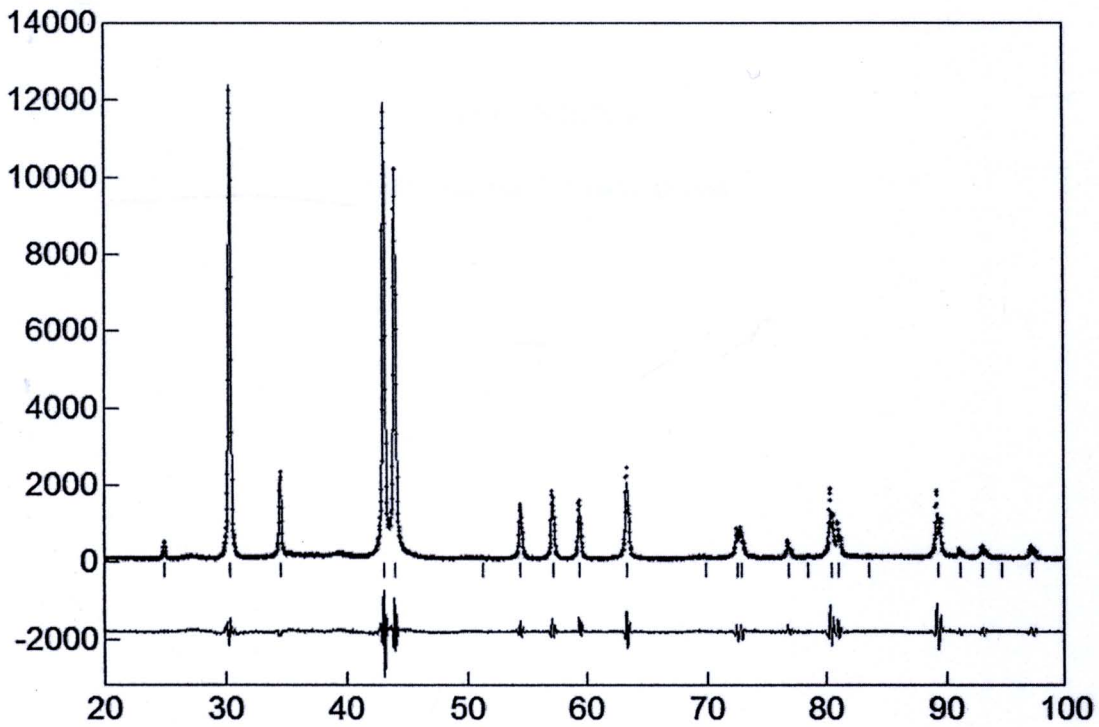

APPENDIX E

International Publications

Materials Letters 63 (2009) 2103–2106

Contents lists available at ScienceDirect

Materials Letters

journal homepage: www.elsevier.com/locate/matlet

Solid-state synthesis of cubic ZnTe nanocrystals using a microwave plasma

Tawat Suriwong [a], Somchai Thongtem [a,*], Titipun Thongtem [b]

[a] Department of Physics and Materials Science, Faculty of Science, Chiang Mai University, Chiang Mai 50200, Thailand
[b] Department of Chemistry, Faculty of Science, Chiang Mai University, Chiang Mai 50200, Thailand

ARTICLE INFO

Article history:
Received 29 May 2009
Accepted 2 July 2009
Available online 18 July 2009

Keywords:
Nanomaterials
Characterization methods
X-ray techniques
Electron microscopy
Luminescence

ABSTRACT

Cubic ZnTe nanocrystals were produced from 1:1 and 1.8:1 molar ratios of Zn:Te by a 900 W microwave plasma. The phase was detected using X-ray diffraction (XRD), which are in accordance with those of the simulations, and selected area electron diffraction (SAED). Raman spectroscopy, scanning electron microscopy (SEM) and transmission electron microscopy (TEM) showed that the products were nanocrystals with different orientations, including three longitudinal optical (LO) vibrations at 205, 410 and 620 cm^{-1} and a transverse optical (TO) vibration at 166 cm^{-1}. Their green emissions were detected at 562 nm (2.21 eV) using luminescence spectrophotometry.

1. Introduction

ZnTe is a II–VI semiconducting material which has a 2.26 eV direct wide band gap at 300 K [1,2] and a 6.2 nm exciton Bohr radius [2]. It has a great deal of potential applications: green-light-emitting diodes, solar cells, waveguides, modulators [1], and other optoelectronic and thermoelectric devices [2]. Previously, ZnTe was successfully produced, such as ZnTe nanowires by oriented attachment [2], highly crystalline ZnTe nanocrystals with controlled shape under different growth conditions [3], ZnTe nanowires by the solution–liquid–solid (SLS) mechanism [4], submicrosized ZnTe rods, ZnO/ZnTe cables and ZnTe tubes via exterior-to-interior boron–chalcogen corrosions on the initial ZnO rods [5], single-crystalline ZnTe nanowire arrays by the pulsed electrochemical deposition from aqueous solutions into porous anodic alumina membranes [6], zinc-blende ZnTe nanostructures, periodically twinned nanowires and uniform nanoribbons by hydrogen-assisted thermal evaporation in the presence of Au catalyst via the vapor–liquid–solid (VLS) growth mechanism [7], multilayer superstructures of single-crystalline ZnTe nanowire films through a new growth process: well-aligned ZnTe nanowires congregate into nanowire films [8], and ZnTe powder by a microwave synthesis under 10^{-6} Torr (1.33×10^{-4} Pa) followed by a ZnTe single crystal growth via the vertical Bridgman method [1]. Microwave radiations (2.45 GHz) are coherent and polarized [1]. They are able to couple with atomic materials, and cause them to be heated up very rapidly. In general, materials are classified into three groups: reflectors (bulk metals and alloys), transparencies (fused-silica and fluoropolymers), and absorbers (inorganic materials, powdered metals, metal oxides and metal halides) [9]. The purpose of the present research was to find the way to save the energy consumption for producing purified ZnTe nanocrystals by a microwave plasma under 4.3 ± 1 kPa argon absolute pressure. This synthetic process required a pressure that is not as low as previously done by Bose et al. [1]. It is inexpensive, shorten reaction time, and environmentally benign.

2. Experiment

To produce ZnTe, Zn and Te powders (purum, analytical grade, Fluka) were used without further purification. Two solid mixtures with 1:1 and 1.8:1 molar ratios of Zn:Te (2 g each) were loaded into silica tubes (11 mm I.D.× 100 mm long), each of which was placed in a horizontal (H) quartz tube. The tube was tightly closed and evacuated to 4.3 ± 1 kPa absolute pressure for removal of air. Subsequently, argon was gradually fed into this H tube. The procedure was repeated three times. Finally, argon in the H tube was evacuated to a constant value of 4.3 ± 1 kPa absolute pressure. Simultaneously, each solid mixture was heated by a 900 W microwave plasma for 10 min, and left to cool down in the vacuum to room temperature. The solid was milled and thoroughly mixed for 5 min. Microwave heating was repeated under the same condition for 10 min at a time, until at the completion of the process. The microwave heating of 1:1 molar ratio products for 10, 20, 30 and 40 min were encoded as A1, A2, A3 and A4, and 1.8:1 molar ratio products for 10 and 20 min as B1 and B2, respectively. The products were then characterized to determine their phase, morphologies, vibrations and emission.

3. Results and discussion

All spectra (Fig. 1a and b) of the products were characterized using XRD and JCPDS database (Reference codes: 15-0746 for ZnTe, 01-1238

* Corresponding author. Tel.: +66 53 941924; fax: +66 53 943445.
E-mail addresses: schthongtem@yahoo.com, sthongtem@hotmail.com (S. Thongtem).

0167-577X/$ – see front matter © 2009 Elsevier B.V. All rights reserved.
doi:10.1016/j.matlet.2009.07.002

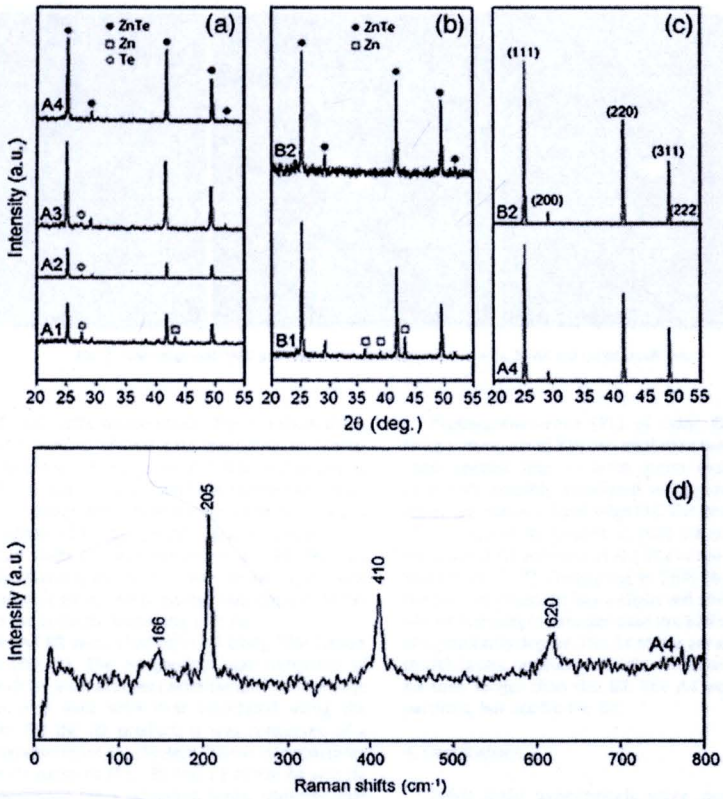

Fig. 1. (a–c) XRD spectra and their simulation, and (d) Raman spectrum of different products.

for Zn and 01-0714 for Te) [10]. At 1:1 molar ratio of Zn:Te and under the 10, 20 and 30 min heating conditions (Fig. 1a), the products (A1, A2 and A3) were composed of ZnTe with some impurities. For 10 min long (A1), both Zn and Te impurities were left in the product. When the reaction time was lengthened to 20 and 30 min, only Te impurity was left in the main products (A2 and A3). No such impurities were detected, when the experimental time was lengthened to 40 min (A4). At the present stage, the chemical reaction of Zn and Te was complete, and only cubic ZnTe was produced as the main product. To save the energy consumption, 1.8:1 molar ratio of Zn:Te (Fig. 1b) was used in the process. ZnTe including some Zn impurity were detected in the product produced under the 10 min heating condition (B1). When the experimental time was lengthened to 20 min (B2), only ZnTe existed as the main products without impurity detection. During the heating process, some of Zn and Te could evaporate as well.

XRD patterns of the A4 and B2 products were also simulated using CaRine Version 3.1 program [11] and Cu–K_α line (0.15406 nm [12]). The results are shown in Fig. 1c. The 2θ diffraction angles and intensities (I) of different crystallographic planes obtained from the experiment, simulation, and the JCPDS database for cubic ZnTe [10] are summarized in Table 1. It is worth noting that these values are in good accordance: simulated patterns for particular conditions were created and used to specify that the experimental patterns could exist in reality, which correspond very well with that of the JCPDS database [10].

Crystallite size (D) of the A4 product was calculated using the (111) peak of its XRD spectrum and the Scherrer's equation [13].

$$D = \frac{K\lambda}{\beta \cos\theta}$$

K is the geometric (shaped) factor which usually takes a value of 0.9 [14,15], λ is the wavelength of Cu K_α radiation (0.15406 nm [12]), and β and θ are the full width at half maximum and Bragg's angle of the (111) peak, respectively. The calculated crystallite size of the A4 product is 77.52 nm.

Table 1
The 2θ diffraction angles (°) and intensities (%) of the JCPDS database for cubic ZnTe, and A4 and B2 products obtained from the experiment (expt.) and simulation (sml.).

Plane	JCPDS		A4 (expt.)		B2 (expt.)		A4 and B2 (sml.)	
	2θ	I	2θ	I	2θ	I	2θ	I
(111)	25.3	100	25.2	100	25.3	100	25.3	100
(200)	29.2	10	29.2	14	29.2	18	29.3	7
(220)	41.8	80	41.9	87	41.9	77	41.9	64
(311)	49.5	35	49.5	53	49.5	61	49.5	38
(222)	51.8	4	51.9	5	51.9	8	51.9	1

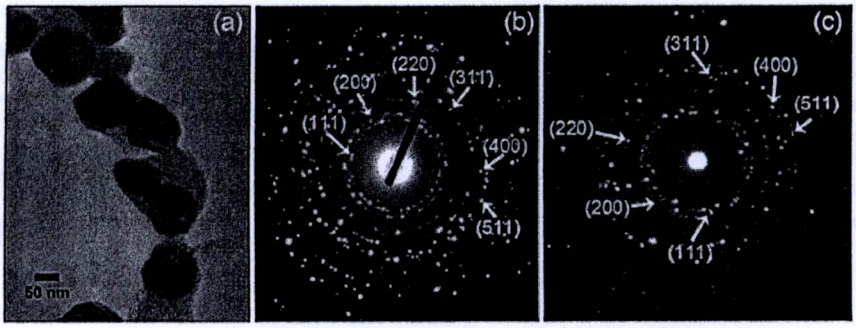

Fig. 2. TEM image and SAED patterns of ZnTe produced under the (a, b) A4 and (c) B2 conditions.

Raman spectrum of cubic ZnTe nanocrystals (Fig. 1d) show three longitudinal optical (LO) modes of 1LO (1st harmonic or fundamental), 2LO (2nd harmonic or 1st overtone) and 3LO (3rd harmonic or 2nd overtone) at 205, 410 and 620 cm^{-1}, and one transverse optical (TO) mode at 166 cm^{-1}, respectively. These Raman shifts are in good accordance with those obtained by Jiang et al. [7], who specified the 1LO, 2LO and TO Raman shifts of ZnTe nanowires at 198, 396 and 168 cm^{-1}, respectively. Comparing to 30 mW He–Ne laser with 632.8 nm (red) wavelength, a great deal of energy was lost during the Raman analysis, due to the inelastic scattering process.

Morphologies of A4 and B2 were characterized using SEM (result not shown) and TEM (Fig. 2). The A4 product was composed of 73.37 nm facet nanoparticles with different orientations. This average size is in accordance very well with that calculated using the Scherrer's equation. But for the B2 product, it was composed of a number of irregular nanoparticles in clusters. These nanoparticles have unclear facets. SAED patterns (Fig. 2b and c) of the A4 and B2 products appear as concentric rings of bright spots, showing that these products were composed of a number of nanocrystals with different orientations. The spaces between adjacent planes were calculated using diameters of the diffraction rings [16], and compared with those of the JCPDS database [10]. The rings for both of these products correspond to the (111), (200), (220), (311), (400) and (511) planes of cubic ZnTe.

Photoluminescence (PL) of cubic ZnTe were studied at room temperature, using 370 nm excitation wavelength from a xenon laser. Their spectra (Fig. 3) were green emission centered at 562 nm (2.21 eV), possibly associated with point defects located at 0.4 eV above the valence band edge [1]. The emission is in accordance with those detected by Jiang et al. (560 nm or 2.21 eV emitted from ZnTe nanowires) [7] and Park et al. (552 nm or 2.25 eV emitted from 14 nm nanocrystals) [3]. Comparing to ZnTe (bulk) with 2.26 eV band gap, the present emission has a slight red shift [7]. It is worth noting that the A4 intensity is stronger than the B2 intensity, due to the difference of crystallinity degree. The A4 atoms are arranged in higher order than the B2 atoms, resulting from the difference in the reaction times – the A4 took longer than the B2. The A4 was composed of facet nanoparticles, but not for the B2.

4. Conclusions

Cubic ZnTe nanocrystals were successfully produced by an inexpensive solid-state synthesis using a 900 W microwave plasma. The phase, nanocrystals, and first three LO and a TO modes for the product with 1:1 molar ratio and 40 min heating were clearly detected. Their photoluminescence was the same green emission centered at 562 nm (2.21 eV), possibly associated with point defects at 0.4 eV above the valence band edge.

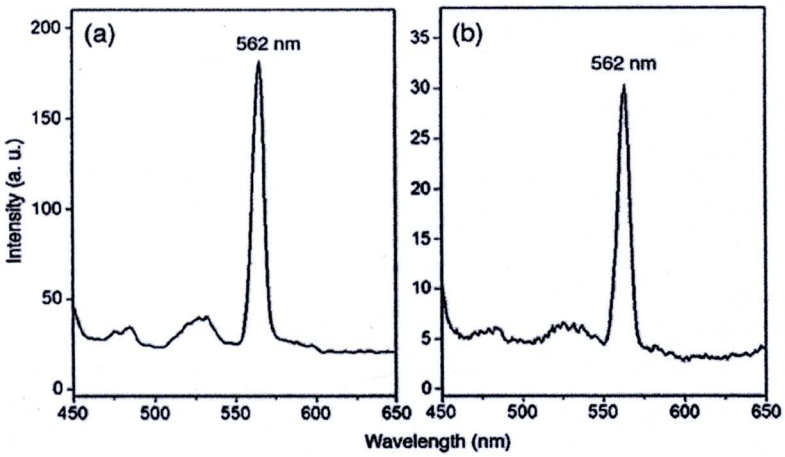

Fig. 3. Photoluminescence of ZnTe produced under the (a) A4 and (b) B2 conditions.

Acknowledgements

We are extremely grateful to the Thailand Research Fund (TRF), Thailand for financial support, and the Graduate School of Chiang Mai University for general funding.

References

[1] Bhunia S, Bose DN. J Cryst Growth 1998;186:535–42.
[2] Yong KT, Sahoo Y, Zeng H, Swihart MT, Minter JR, Prasad PN. Chem Mater 2007;19:4108–10.
[3] Lee SH, Kim YJ, Park J. Chem Mater 2007;19:4670–5.
[4] Fanfair DD, Korgel BA. Cryst Growth Des 2008;8:3246–52.
[5] Huang YZ, Chen L, Wu LM. Inorg Chem 2008;47:10723–8.
[6] Li L, Yang Y, Huang X, Li G, Zhang L. J Phys Chem, B 2005;109:12394–8.
[7] Meng Q, Jiang C, Mao SX. J Cryst Growth 2008;310:4481–6.
[8] Guo Y, Geng B, Zhang L, Zhan F, You J. J Phys Chem, C 2008;112:20307–11.
[9] Lekse JW, Pischera AM, Aitken JA. Mater Res Bull 2007;42:395–403.
[10] Powder Diffract. File, JCPDS-ICDD, 12 Campus Boulevard, Newtown Square, PA 19073-3273, U.S.A.; 2001.
[11] Boudias C, Monceau D. CaRIne Crystallography 3.1, DIVERGENT S.A., Centre de Transfert, 60200 Compiègne, France; 1989–1998.
[12] Mastrovito C, Lekse JW, Aitken JA. J Solid State Chem 2007;180:3262–70.
[13] Suryanarayana C, Norton MG. X-ray Diffract., A Pract. Appro. New York: Plenum Press; 1998.
[14] Yang L, Shen Q, Zhou J, Jiang K. Mater Chem Phys 2006;98:125–30.
[15] Hong YC, Uhm HS. Chem Phys Lett 2006;422:174–8.
[16] Andrews KW, Dyson DJ, Keown SR. Interpret. Electr. Diffract. Patterns. New York: Plenum Press; 1971.

Journal of Alloys and Compounds 509 (2011) 4014–4017

Contents lists available at ScienceDirect

Journal of Alloys and Compounds

journal homepage: www.elsevier.com/locate/jallcom

Synthesis and high-temperature thermoelectric properties of Ni_3GaSb and Ni_3InSb

Tawat Suriwong[a], Ken Kurosaki[b,*], Somchai Thongtem[a], Adul Harnwunggmoung[b], Tohru Sugahara[b], Theerayuth Plirdpring[b], Yuji Ohishi[b], Hiroaki Muta[b], Shinsuke Yamanaka[b,c]

[a] Department of Physics and Materials Science, Faculty of Science, Chiang Mai University, Chiang Mai 50200, Thailand
[b] Graduate School of Engineering, Osaka University, Suita 565-0871, Japan
[c] Research Institute of Nuclear Engineering, University of Fukui, Fukui 910-8507, Japan

ARTICLE INFO

Article history:
Received 1 December 2010
Received in revised form 1 January 2011
Accepted 3 January 2011
Available online 6 January 2011

Keywords:
Ni_3GaSb
Ni_3InSb
Thermoelectric
Seebeck coefficient
Electrical resistivity
Thermal conductivity

ABSTRACT

Ni_3GaSb and Ni_3InSb were successfully synthesized by the direct reaction of Ni and GaSb or InSb. The XRD patterns and the lattice parameters of these compounds were in good agreement with the literature data. The Seebeck coefficient (S), the electrical resistivity (ρ), and the thermal conductivity (κ) of Ni_3GaSb and Ni_3InSb were examined in the temperature range from room temperature to 1073 K. Both compounds indicated metal-like characteristics. The power factor ($S^2\rho^{-1}$) values increased with temperature and reached maximum at 1073 K. The κ and the dimensionless figure of merit ZT of both samples increased with temperature. The maximum values of the ZT of Ni_3GaSb and Ni_3InSb were obtained at 1073 K to be 0.022 and 0.023, respectively.

1. Introduction

The thermoelectric (TE) technology, used for direct conversion of waste heat into electrical power is expected to substantially contribute to future power supply and sustainable energy management [1,2]. The efficiency of a material used in TE devices is determined by the dimensionless figure of merit, $ZT = S^2T/\rho/\kappa$, where S, ρ, T, and κ are the Seebeck coefficient, electrical resistivity, absolute temperature, and thermal conductivity. In order to maximize ZT of the material, S is required to be the highest, but ρ and κ are the lowest. Due to their transport property interrelation, they are needed to be optimized to achieve maximum ZT. In recent years, several classes of bulk materials [3,4] with high ZT were discovered, including those found for new TE materials [5,6].

Among the III–V binary semiconductors, gallium antimonide (GaSb) and indium antimonide (InSb) have attracted considerable attention over the last several years. GaSb based binary and ternary alloys have turned out to be important candidates for applications in long wavelength lasers and photodetectors for fiber optic communications [7]. InSb has been interested in high speed applications for transistors and other devices [8,9], which is associated directly with the very low electron effective mass and high mobility [10].

Based on these interesting electrical properties, the TE properties such as S, ρ, and κ of GaSb and InSb have been examined [11–14]. For example, Su et al. investigated the TE properties of Zn-doped InSb single crystals and reported the maximum ZT value to be around 0.27 at 700 K [13]. The TE properties of In_2Te_3–InSb solid solutions were also examined [14]. Ebnalwaled investigated the TE properties of GaSb bulk crystals and reported the power factor value (8.82×10^{-3} mW m^{-1} K^{-2} at 322 K) [11]. However, as for ternary compounds containing Ga, In, and Sb, the TE properties have scarcely reported.

As for M-(Ga or In)–Sb ternary compounds, the existing of Ni_3GaSb and Ni_3InSb have been reported by Jan and Chang [15]. These compounds exhibit the hexagonal, $P63/mmc$ crystal structure – similar to that of Ni_3GaAs [16]. The melting points were determined to be >1339 K and >1364 K for Ni_3GaSb and Ni_3InSb, respectively [15]. However, the physical properties including the TE properties of these compounds are unknown at this moment. In the present study, therefore, we tried to synthesize Ni_3GaSb and Ni_3InSb and investigate the TE properties from room temperature to 1073 K.

2. Experimental

The Ni_3GaSb and Ni_3InSb ternary compounds were synthesized by direct reactions of mixtures of the stoichiometric ratios of Ni (3 N), GaSb (6 N), and InSb (5 N) in sealed silica tubes. These mixtures were processed in a series of steps: preheated at 973 K for 12 h, slowly heated up to 1323 K for 3 days, rapidly cooled to 973 K

* Corresponding author. Tel.: +81 6 6879 7905; fax: +81 6 6879 7889.
E-mail address: kurosaki@see.eng.osaka-u.ac.jp (K. Kurosaki).

0925-8388/$ – see front matter © 2011 Elsevier B.V. All rights reserved.
doi:10.1016/j.jallcom.2011.01.006

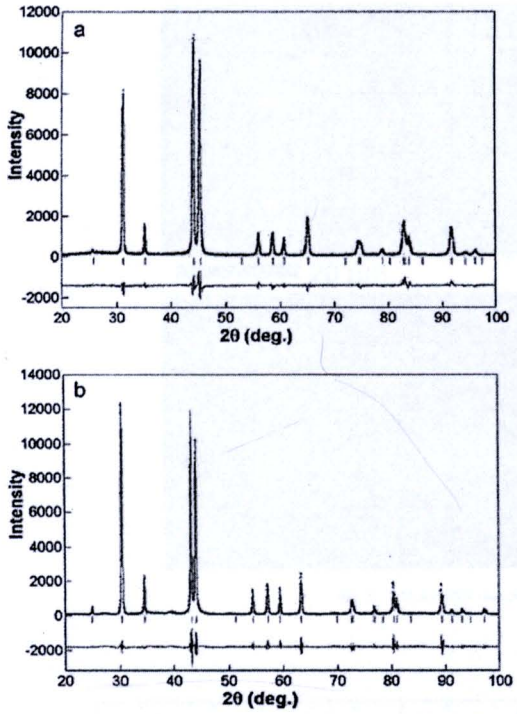

Fig. 1. Powder XRD patterns of the polycrystalline samples and the results of the Rietveld refinement of (a) Ni_3GaSb and (b) Ni_3InSb. The experimental data are shown as small red crosses, the calculated fits and the difference curves are shown as blue solid lines. Short vertical lines (green) below the patterns indicate the calculated peak positions. (For interpretation of the references to color in this figure legend, the reader is referred to the web version of this article.)

and held at this temperature for 4 days, and quenched in an ice water bath. The products were crushed and milled into fine powders. Bulk samples were then produced by spark plasma sintering (DR.SINTER LAB, SPS-515A) of the fine powders in a 20 mm diameter graphite die using 40 MPa sintering pressure at 1123 K for 30 min in an argon-flow atmosphere. The ingots were cut into the rectangular shapes of 3 mm × 3 mm × 15 mm and 10 mm × 10 mm × 1 mm. Their phases, morphologies, and chemical compositions were characterized by a powder X-ray diffraction (XRD) technique using Cu Kα radiation in a step scan condition (fixed time) with an increment of 0.02° and a slit-condition of 1.0°–1.0°–0.60 mm (DS–SS–RS) on Rigaku RINT 2000, and a scanning electron microscope (SEM) equipped with an energy dispersive X-ray (EDX) analyzer (Hitachi, S2600H) at room temperature. The density of the bulk samples was calculated based on the measured weight and dimensions. The electrical resistivity (ρ) and the Seebeck coefficient (S) were measured using a commercially available apparatus (ULVAC, ZEM-1) in a helium atmosphere. Thermal conductivity (κ) was evaluated from thermal diffusivity (α), heat capacity (C_p) and sample density (d) based on the relationship $\kappa = \alpha C_p d$. The thermal diffusivity was measured under vacuum by the laser flash apparatus (ULVAC, TC-7000). C_p was estimated from the Dulong–Petit model, $C_p = 3nR$, where n is the number of atom per formula unit and R is the gas constant. The TE properties were evaluated in the temperature range from room temperature to 1073 K.

3. Results and discussion

The powder XRD patterns of the prepared samples are shown in Fig. 1. Both the samples were identified as Ni_3GaSb and Ni_3InSb, according to the JCPDS database (Reference codes: 47-1401 for Ni_3GaSb and 47-1402 for Ni_3InSb) [15,17], although these compounds contained a few peaks that were inconsistent with the JCPDS data. Therefore, the XRD experimental data were analyzed by the Rietveld refinement [18] on the X-ray diffraction patterns, using

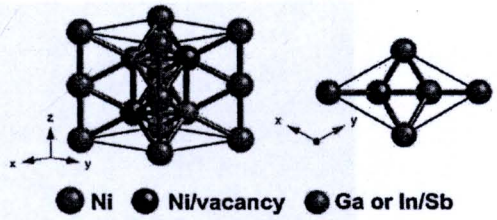

Fig. 2. Crystal structure of Ni_3GaSb and Ni_3InSb.

the hexagonal crystal system with the space group of $P63/mmc$. Details of the structure are reported in Ref. [15]. Refinement of the patterns for both compounds revealed that all the reflections can be indexed to the Ni_3GaSb and Ni_3InSb phases with no evidence of the impure phases.

The crystal structure of the compounds is described in Fig. 2. According to the crystal structure of Ni_3GaAs [16], Ni atoms occupy the (0, 0, 0) and the (0, 0, 1/2) positions; one vacancy and one Ni atom randomly occupy the (2/3, 1/3, 1/4) and the (1/3, 2/3, 3/4) positions; and Ga and As atoms randomly occupy the (1/3, 2/3, 1/4) and the (2/3, 1/3, 3/4) positions. The results of the Rietveld analysis for Ni_3GaSb and Ni_3InSb were in good agreement with the results of the crystal structure analysis of Ni_3GaAs.

The lattice parameters, sample bulk density, and chemical composition of the samples are summarized in Table 1. The hexagonal lattice parameters and the theoretical density of these compounds were in good agreement with those reported by Jan and Chang [15]. The densities of the polycrystalline samples taken from the sintered specimens for TE characterizations were 96% of the theoretical density. All the samples appeared to be stable in air at room temperature. The quantitative EDX analysis confirmed that the chemical compositions of the bulk sintered samples corresponded to the stoichiometric compositions, as summarized in Table 1.

The SEM and EDX mapping images of the bulk Ni_3GaSb sample are shown in Fig. 3. The SEM image indicated that the sample was homogeneous. The EDX analysis revealed that Ni, Ga, and Sb were uniformly distributed on the sample surface. As for Ni_3InSb, similar results to those for Ni_3GaSb were obtained; i.e. the SEM and EDX analyses confirmed that the Ni_3GaSb and the Ni_3InSb samples were homogeneous with stoichiometric chemical composition.

The temperature dependences of the electrical properties of the Ni_3GaSb and the Ni_3InSb samples are shown in Fig. 4. The electrical resistivity (ρ) of both samples exhibited a metal-like behavior; increased with temperature in the whole temperature range and

Table 1
Lattice parameters, sample bulk density, and chemical composition of Ni_3GaSb and Ni_3InSb.

	Ni_3GaSb	Ni_3InSb
Lattice parameter		
$a = b$ (Å)	4.0135 [4.0000]	4.1111 [4.1100]
c (Å)	5.1136 [5.0900]	5.1882 [5.1900]
Theoretical density		
d_{th} (g cm^{-3})	8.56 [8.65]	8.97 [9.03]
Measured density		
d_{exp} (g cm^{-3})	8.18	8.60
Relative density		
$d_{exp/dth} \times 100$ (%)	96	96
Chemical composition determined through the EDX analysis (at.%)		
Ni	59.5	59.9
Ga	20.1	–
In	–	20.0
Sb	20.4	20.1

[], Ref. [15].

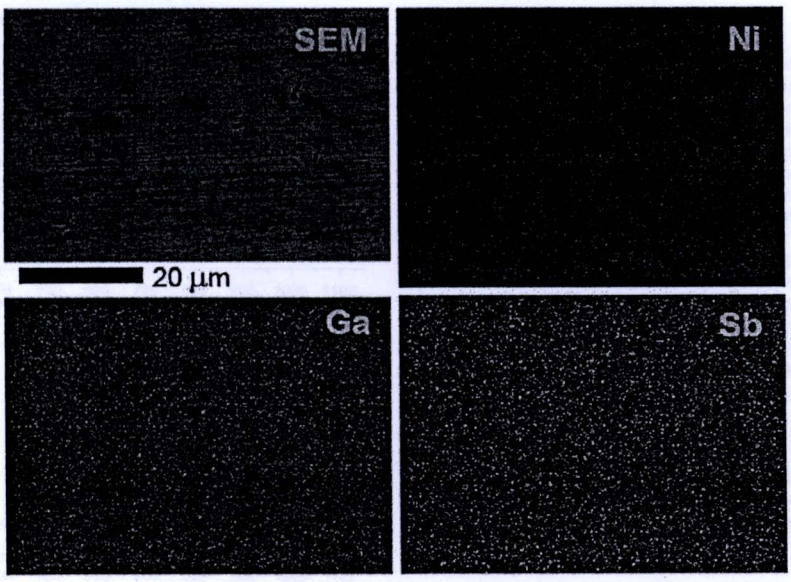

Fig. 3. SEM and EDX mapping images of the Ni_3GaSb bulk sample.

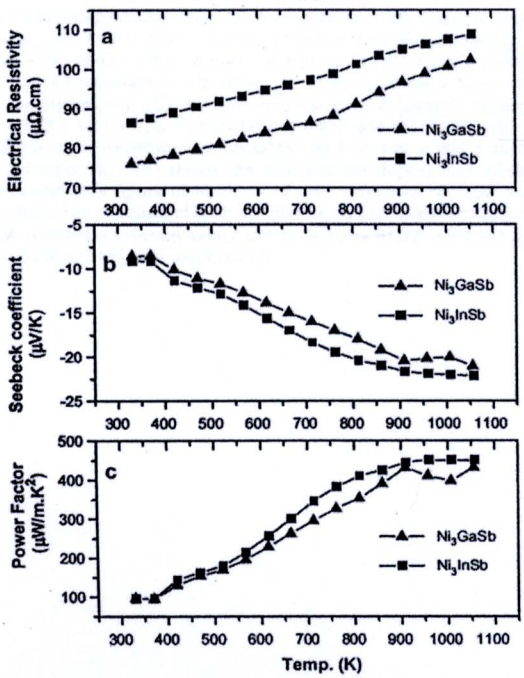

Fig. 4. Temperature dependences of the electrical properties of the polycrystalline samples Ni_3GaSb and Ni_3InSb; (a) electrical resistivity ρ, (b) Seebeck coefficient S, and (c) power factor $S^2\rho^{-1}$.

reached a maximum at 1073 K, as shown in Fig. 4(a). The Seebeck coefficient (S) values were negative for both samples, as shown in Fig. 4(b), indicating that the majority of charge carriers were electrons. The absolute S values of these samples increased with temperature and kept a constant at around 900–1073 K. The absolute S values were quite low like metals; the S values of Ni_3GaSb and Ni_3InSb at 1073 K were −21 and −22 $\mu V\,K^{-1}$, respectively. Ni_3GaSb exhibited the lower ρ and the lower absolute S values than those of Ni_3InSb. Since the larger carrier concentration (n) basically leads to the lower ρ and the lower absolute S, Ni_3GaSb would have the larger n values than that of Ni_3InSb. In order to discuss the magnitude relationship in the electrical properties in more detail, the Hall measurements should be performed. The power factor ($S^2\rho^{-1}$) data of the samples are plotted in Fig. 4(c), as a function of temperature. The power factor was increased with temperature and kept a constant at around 900–1073 K. The maximum values of the power factor of Ni_3GaSb and Ni_3InSb were obtained at 1073 K to be 0.43 and 0.45 $mW\,m^{-1}\,K^{-2}$, respectively. These values were larger than those of the related compounds such as pure GaSb [11] and InSb [12] bulk samples.

The temperature dependence of the thermal conductivity (κ) of the polycrystalline samples of Ni_3GaSb and Ni_3InSb is shown in Fig. 5(a). Unfortunately, the κ values of both samples were quite high like metals and increased with temperature. Ni_3GaSb presented the higher κ values than Ni_3InSb because of the larger electronic contribution on κ of Ni_3GaSb than that of Ni_3InSb. The lattice thermal conductivity κ_{lat} was obtained by subtracting the electronic thermal conductivity κ_{el} from the total (measured) thermal conductivity κ. The value of κ_{el} was calculated using $\kappa_{el} = L\sigma T$, where σ is the electrical conductivity ($=1/\rho$) and L is the Lorentz number ($L = 2.45 \times 10^{-8}\,W\Omega\,K^{-2}$). Room temperature values of the κ_{lat} for Ni_3GaSb and Ni_3InSb were 3.2 and 2.3 $Wm^{-1}\,K^{-1}$, respectively. These relatively low κ_{lat} of Ni_3GaSb and Ni_3InSb would be caused by their complex crystal structure containing a lot of vacancies as described previously. The heavier molecular weight of Ni_3InSb than that of Ni_3GaSb would lead to the lower κ_{lat} of Ni_3InSb than that of Ni_3GaSb. Note that here the calculated κ_{el}

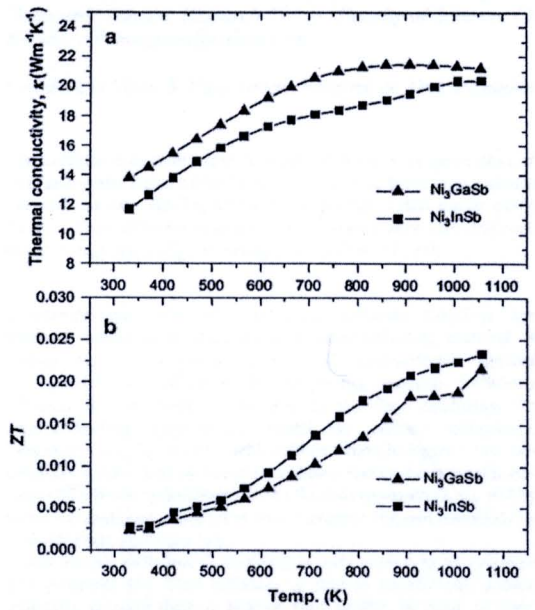

Fig. 5. Temperature dependences of the (a) thermal conductivity κ and (b) dimensionless figure of merit ZT of the polycrystalline samples of Ni_3GaSb and Ni_3InSb.

exhibited larger values than the measured κ at high temperatures, i.e. $\kappa_{lat} < 0$. This is likely due to (1) the sample for measuring ρ and κ is not the same sample, i.e. one is 3 mm × 3 mm × 15 mm for ρ measurements, the other is 10 mm × 10 mm × 1 mm for κ measurements; (2) at high temperature the Lorentz number ($L = 2.45 \times 10^{-8}\ W\Omega\ K^{-2}$) may be not valid; and (3) there exists a difference in experimental uncertainties between ρ and κ measurements. Fig. 5(b) shows the temperature dependence of the dimensionless figure of merit ZT of the samples of Ni_3GaSb and Ni_3InSb. The ZT values of both samples increased with temperature and reached maximum values at 1073 K to be 0.022 and 0.023 for Ni_3GaSb and Ni_3InSb, respectively.

4. Summary

In the present study, Ni_3GaSb and Ni_3InSb were successfully synthesized and the electrical resistivity (ρ), the Seebeck coefficient (S), and the thermal conductivity (κ) were examined from room temperature to 1073 K. The XRD patterns and the lattice parameters were in good agreement with the previously reported data. The crystal structure was hexagonal with the space group of $P63/mmc$. The ρ of both compounds increased with temperature, indicating a metal-like behavior. The S values were negative for both samples and the absolute values were low ($<10\ \mu V\ K^{-1}$ at room temperature for both compounds) like metals. Ni_3GaSb exhibited the lower ρ and absolute S values than those of Ni_3InSb, most likely due to the larger carrier concentration of Ni_3GaSb than that of Ni_3InSb. The κ and the ZT values of both samples were increased with temperature. The maximum values of the ZT of Ni_3GaSb and Ni_3InSb were obtained at 1073 K to be 0.022 and 0.023, respectively.

Acknowledgments

We are grateful to the Thailand Research Fund (TRF) through Royal Golden Jubilee Ph.D. Program (RGJ-Ph.D.); grant number PHD/0078/2550, Thailand for financial support, and the Graduate School of Chiang Mai University for general funding.

References

[1] T.M. Tritt, M.A. Subramanian, MRS Bull. 31 (2006) 188.
[2] D.M. Rowe (Ed.), CRC Handbook of Thermoelectrics, CRC Press, New York, 1995.
[3] G.J. Snyder, E.S. Toberer, Nat. Mater. 7 (2008) 105.
[4] H. Kleinke, Chem. Mater. 22 (2010) 604.
[5] J.P. Heremans, V. Jovovic, E.S. Toberer, A. Saramat, K. Kurosaki, A. Charoenphaldee, S. Yamanaka, G.J. Snyder, Science 321 (2008) 554.
[6] K. Kurosaki, A. Kosuga, H. Muta, M. Uno, S. Yamanaka, Appl. Phys. Lett. 87 (2005) 061919.
[7] F. Capasso, M.B. Panish, S. Sumski, P.W. Foy, Appl. Phys. Lett. 36 (1980) 165.
[8] R.G. van Welzenis, B.K. Ridley, Solid State Electron. 27 (1984) 113.
[9] R.J. Egan, V.W.L. Chin, T.L. Tansley, Semicond. Sci. Technol. 9 (1994) 1591.
[10] N.K. Udayashankar, H.L. Bhat, Bull. Mater. Sci. 24 (2001) 445.
[11] A.A. Ebnalwaled, Mater. Sci. Eng. B 174 (2010) 285.
[12] A.A. Ebnalwaled, J. Cryt. Growth 311 (2009) 4385.
[13] X.L. Su, H. Li, X.F. Tang, J. Phys. D: Appl. Phys. 43 (2010) 015403.
[14] Y. Pei, D.T. Morelli, Appl. Phys. Lett. 94 (2009) 122112.
[15] C.H. Jan, Y.A. Chang, J. Mater. Res. 6 (1991) 2660.
[16] T. Sands, V.G. Keramidas, J. Washburn, R. Gronsky, Appl. Phys. Lett. 48 (1986) 402.
[17] Powder Diffract. File, JCPDS-ICDD, 12 Campus Boulevard, Newtown Square, PA 19073-3273, USA, 2001.
[18] F. Izumi, K. Momma, Solid State Phenom. 130 (2007) 15–20.

Direct energy gap of Sb_2Te_3 synthesised by solid-state microwave plasma

T. Suriwong[1], *T. Thongtem*[2,3], *S. Thongtem*[1,3]

[1]*Department of Physics and Materials Science, Faculty of Science, Chiang Mai University, Chiang Mai 50200, Thailand*
[2]*Department of Chemistry, Faculty of Science, Chiang Mai University, Chiang Mai 50200, Thailand*
[3]*Materials Science Research Center, Faculty of Science, Chiang Mai University, Chiang Mai 50200, Thailand*
E-mail: schthongtem@yahoo.com

Published in Micro & Nano Letters; Received on 22nd September 2010; Revised on 25th January 2011

The usefulness of microwave heating and microwave generation of plasma for solid-state synthesis of Sb_2Te_3 crystals is reported. Lengths of time and molar ratios of Sb:Te were varied to achieve pure products heated by a 900 W microwave-irradiated plasma. In the present research, the products were Sb_2Te_3 with a rhombohedral crystal system using 2:2, 2:1.75 and 2:1.5 molar ratios of Sb:Te, and lengths of time of 10 and 20 min. Their different crystallographic planes were also detected, including four Raman shifts at 93.9, 102.6, 139.2 and 263.7 cm^{-1}, and direct energy gaps (E_g) in a range of 0.340–0.515 eV.

1. Introduction: Recently, antimony telluride (Sb_2Te_3) has received considerable attention as a semiconducting material of interest for use in optoelectronic and thermoelectric devices [1, 2], which are influenced by the energy bandgap. Antimony telluride is considered to be one of the best candidates for semiconducting applications based on current technology. Previously, Sb_2Te_3 crystals with different morphologies were successfully synthesised by chemical solution routes: hexagonal nanoplates by a facile hydrothermal/solvothermal approach [2, 3], and by refluxing synthesis using microwave radiation [4]; and nanobelts by hydrothermal synthesis [5].

Microwave radiation (2.45 GHz) is well known to be coherent and polarised [6]. This radiation is able to couple with atomic materials, causing them to heat up very rapidly. In terms of interaction with microwave irradiation, materials are classified into three groups: reflectors (bulk metals and alloys), transmitting materials (fused-silica and fluoropolymers) and absorbers (inorganic materials, powdered metals, metal oxides and metal halides) [7]. Our motivation here was to investigate the structure and energy bandgap (E_g) of antimony telluride, synthesised by a solid-state microwave plasma process.

2. Experiment: Sb and Te powders (purum, analytical grade, Fluka) for experimental synthesis were used without further purification. Different molar ratios of Sb:Te (2:3, 2:2.25, 2:2, 2:1.75 and 2:1.5) were loaded into 11 mm I.D. × 100 mm-long silica tubes. Each was then placed in a horizontal quartz tube (Fig. 1), which was tightly closed and evacuated to 4.3 ± 1 kPa absolute pressure. Argon was gradually fed into this quartz tube. Evacuation was repeated three times. Finally, each solid mixture was heated by a 900 W irradiated microwave plasma for 10, 20 and 40 min at 4.3 ± 1 kPa absolute pressure, and left to cool down to room temperature.

Products were characterised and recorded on a Philips X'Pert MPD X-ray diffractometer (XRD) equipped with a graphitic monochromator of Cu-K_α radiation ($\lambda = 0.154056$ nm), using a scanning rate of 0.02 deg/s over the 2θ range of 10–60°. Raman vibrations of the products were detected by a HORIBA JOBIN YVON T64000 Raman spectrometer with 30 mW and 632.8 nm (red) wavelength He-Ne laser. Field-emission scanning electron microscopic (FESEM) image was taken by a JEOL JSM-6335F operated at 15.0 kV beam energy. Transmission electron microscopic (TEM) images, and selected area electron diffraction (SAED) patterns were taken on a JEOL JEM-2010, employing at an accelerating voltage of 200 kV. Ultraviolet (UV)-visible spectra were carried out by a Lambda 25 spectrometer using UV lamp with the resolution of 1 nm at room temperature.

3. Results and discussion: XRD spectra (Fig. 2) of the products synthesised using 900 W microwave plasma (at different molar ratios of Sb:Te and lengths of time) were compared with the JCPDS database [8]. At a 2:3 molar ratio of Sb:Te, for 10 and 20 min, the products were Sb_2Te_3 (JCPDS no. 15-0874) containing some Te residue (JCPDS no. 36-1452). This residue still remained in the product, even after lengths of time as long as 40 min. The amount of Te was reduced in a series of steps until – at 2:2, 2:1.75 and 2:1.5 molar ratios of Sb:Te, with lengths of time of 10 and 20 min – the products were Sb_2Te_3, without any residual detection. At these stages, Sb and Te had completely combined together chemically to form Sb_2Te_3 with a rhombohedral crystal system and R-3 m space group [8]. During microwave plasma heating, some of the Sb and Te could evaporate as well.

In the present research, approximate crystallite sizes (L) of Sb_2Te_3 crystals synthesised under different conditions were calculated using the Scherrer formula [9]

$$L = \frac{\lambda k}{B \cos \theta} \quad (1)$$

where λ, θ, k and B are (respectively): the wavelength of Cu-K_α radiation (0.154056 nm); Bragg angles of the (015) peaks; a

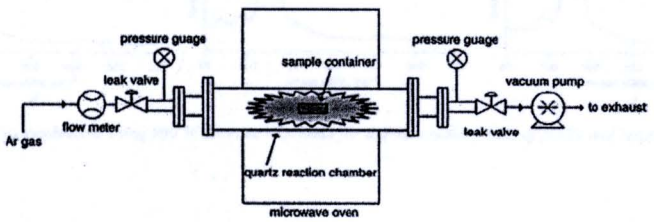

Figure 1 *Schematic diagram of the apparatus used for the Sb_2Te_3 synthesis*

doi: 10.1049/mnl.2010.0227

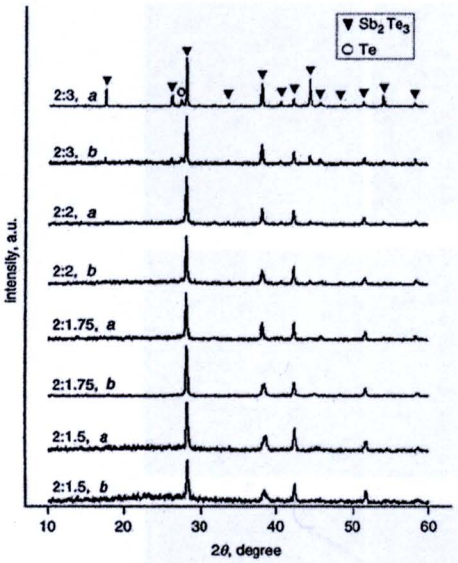

Figure 2 *XRD spectra of the products synthesised using 900 W microwave plasma at different molar ratios of Sb:Te*
a For 10 min
b For 20 min

constant (0.90) and full widths at half maximum of the peaks. Calculated crystallite sizes of Sb_2Te_3 crystals synthesised by the 900 W microwave plasma at different molar ratios of Sb:Te and lengths of time are shown in Table 1. The crystallite sizes increased by 28–43% by increasing the lengths of time from 10 to 20 min with the microwave power remaining at 900 W; sizes increased by 27% and 36% by changing the Sb:Te molar ratios from 2:1.50 to 2:2 with the lengths of time remaining at 10 and 20 min, respectively. These results implied that the molar ratios and lengths of reaction time played key roles in the phase and crystallite sizes of Sb_2Te_3 crystals.

Table 1 Crystallite sizes, and direct energy bandgaps of Sb_2Te_3 crystals synthesised at different Sb:Te molar ratios and lengths of time by 900 W microwave plasma

Sb:Te molar ratio	Length of time, min	Crystallite size, nm	E_g, eV
2:1.50	10	85.8	0.515
2:1.50	20	110.0	0.515
2:1.75	10	88.8	0.515
2:1.75	20	127.3	0.515
2:2	10	109.2	–
2:2	20	150.1	0.340

To further ascertain the presence of Sb_2Te_3, the products were characterised using Raman spectroscopy. Fig. 3 shows four Raman shifts of Sb_2Te_3 crystals at 93.9, 102.6, 139.2 and 263.7 cm^{-1}. These peaks are in good accordance with those of pure Sb_2Te_3 characterised by Zheng *et al.* [10]. Compared to a 30 mW He-Ne laser with 632.8 nm (red) wavelength, a great deal of energy was lost during Raman analysis, caused by the inelastic scattering process.

SAED patterns (Figs. 4*a*, *b*, *d* and *g*) of the products, synthesised under different conditions, are composed of several concentric rings of diffuse spots caused by the diffraction of transmitted electrons through a number of crystals with different orientations. These interpreted patterns [11] were in accordance with a rhombohedral Sb_2Te_3 crystal system [8]. It should be noted that no detection of Te was found in the SAED pattern for a 2:2.25 molar ratio of Sb:Te and 20 min (Fig. 4*g*), although the residue for this same condition was detected by XRD (result not shown). Its concentration could be too low to be detected by the analysis. A typical example of a SEM image of Sb_2Te_3, produced from a 2:1.5 molar ratio of Sb:Te for 20 min, is shown in Fig. 4*c*. This product is composed of a number of nanocrystals with different orientations. A number of crystallographic planes with different orientations of different products (Figs. 4*e*, *f*, *h* and *i*) were also detected by high-resolution TEM (HRTEM). Their spaces correspond to those of the JCPDS database for a rhombohedral Sb_2Te_3 crystal system [8], showing the presence of crystals with different orientations composing the polycrystalline products. Compared with synthesis by other methods, there are some differences in Sb_2Te_3 products: hexagonal nanoplates by hydrothermal/solvothermal reactions

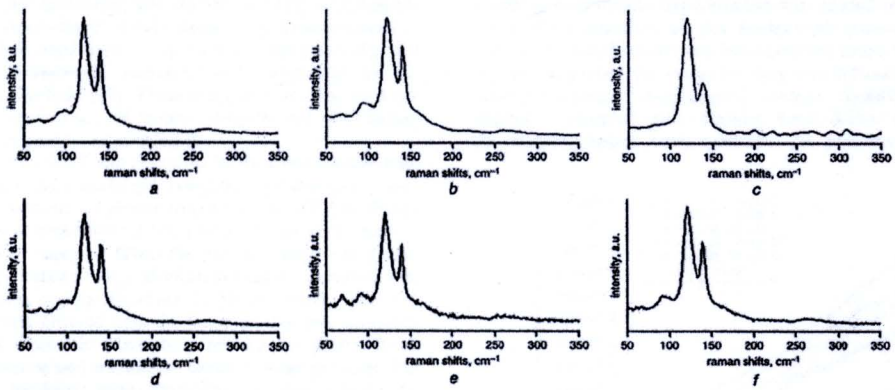

Figure 3 *Raman spectra of Sb_2Te_3 synthesised using 900 W microwave plasma for different molar ratios of Sb:Te and lengths of time*
a 2:1.5, 10 min
b 2:1.5, 20 min
c 2:1.75, 10 min
d 2:1.75, 20 min
e 2:2, 20 min
f 2:2.25, 20 min

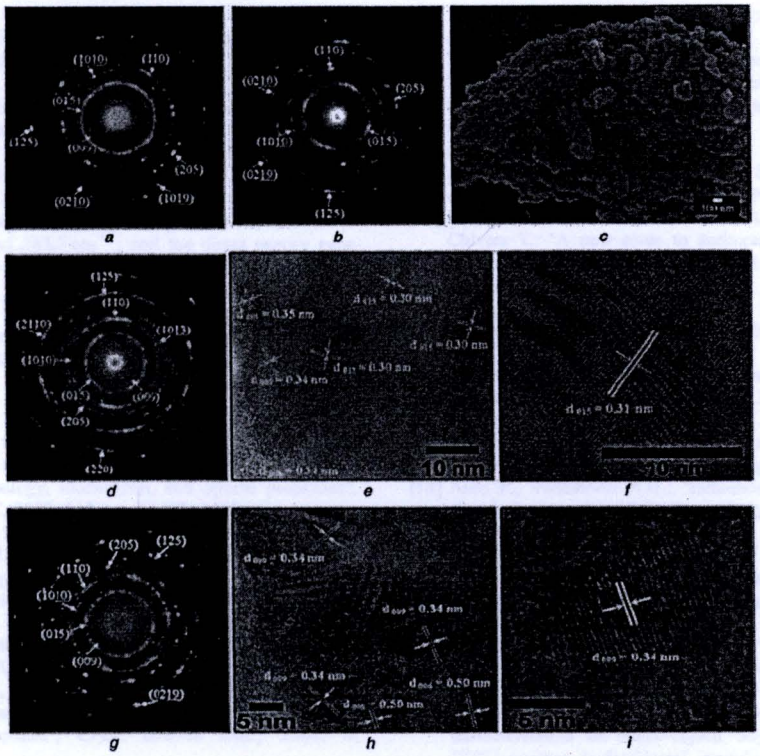

Figure 4 *SAED patterns, and SEM and HRTEM images of Sb_2Te_3 synthesised using 900 W microwave plasma for different molar ratios of Sb:Te and lengths of time*
a 2:1.5, 10 min
b and *c* 2:1.5, 20 min
d–f 2:2, 20 min
g–i 2:2.25, 20 min

[2, 3], microwave-assisted synthesis [4] and aerosol-assisted chemical vapour deposition [12]; nanobelts by a hydrothermal process [5]; nanowire arrays using a porous anodic alumina membrane as a template by electrochemical deposition [13]; single-crystal nanowires by vapor–liquid–solid method [14]; films produced in a dense plasma-focused device [15]; thermal evaporation [16] and nanostructures (nanowires, nanobelts and nanotubes) by the vapour-transport method [17]. These analyses prove that synthesis methods, starting reagents, pH values, templates and other factors can play roles in product morphologies.

Fig. 5 shows the $(\alpha h\nu)^2$ and $(h\nu)$ plots for the direct allowed transition, where α, h and ν are (respectively) the total absorption coefficient, Planck constant and photon frequency [18–20]. The change of absorption was controlled by two photon energy ($h\nu$) ranges – the high and low energies. When the photon energy was greater than the energy bandgap (E_g), absorption linearly increased with increasing photon energy. However for photon energy less than E_g, the absorption differed from the linearity; this was caused by the dominant electronic absorption relating to defect levels between the valence and conduction bands of these products. The direct energy bandgaps were determined by extrapolating the linear parts of these curves to $\alpha = 0$, at which the absorption went to zero with a range of 0.340–0.515 eV (as shown in Table 1). These direct bandgaps are in accordance with those in the 0.29–0.46 eV range for Sb_2Te_3 nanofilms with a thickness between 61.2 nm (35 min deposition) and 4.1 nm (10 min deposition) as determined by Erdoğan and Demir [21], and 0.42 eV for the 400-cycle Sb_2Te_3 film (190 nm thick) as determined by Yang *et al.* [22]. In the case of the last product (2:2 molar ratio of Sb:Te for 20 min), the E_g was reduced to be 0.340 eV. Possibly, undetectable impurities/residues existed in the product. These direct bandgaps are the fundamental parameters used to control the optoelectronic and thermoelectric properties of Sb_2Te_3 crystals. In general, the energy bandgap was influenced by the processing syntheses, morphologies, average crystallite sizes and degrees of structural order–disorder. Some defects could form in the crystalline lattice during synthesis. This promoted the presence

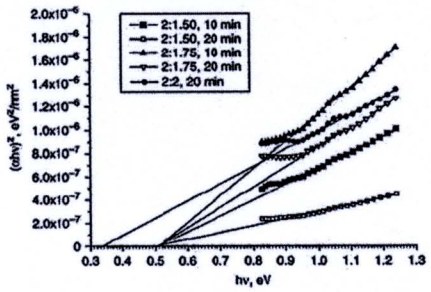

Figure 5 *$(\alpha h\nu)^2$ against $(h\nu)$ plots of Sb_2Te_3, synthesised at different Sb:Te molar ratios and lengths of time by 900 W microwave plasma*

doi: 10.1049/mnl.2010.0227

of intermediate levels between the valence and conduction bands, which can play a role in the bandgap of the products, as well as in their optoelectronic and thermoelectric properties.

4. Conclusions: Sb_2Te_3 with a rhombohedral crystal system was successfully synthesised by an environmentally benign process with a short reaction time using a 900 W irradiated microwave plasma. At 2:2, 2:1.75 and 2:1.5 molar ratios of Sb:Te, with time lengths of 10 and 20 min, the products were pure Sb_2Te_3 phase with no detection of any residue. Their four Raman shifts were at 93.9, 102.6, 139.2 and 263.7 cm^{-1}, and the direct energy gaps were determined to be 0.340–0.515 eV.

5. Acknowledgment: We wish to give thank the Thailand's Office of the Higher Education Commission for providing financial support through the National Research University Project.

6 References

[1] Zhang A., Ma Q., Lu M., Zhou G., Li C., Wang Z.: 'Nanocrystalline metal chalcogenides obtained open to air: synthesis, morphology, mechanism, and optical properties', *J. Phys. Chem. C*, 2009, 113, pp. 15492–15496

[2] Yuan Q., Nie Q., Huo D.: 'Preparation and characterization of the antimony telluride hexagonal nanoplates', *Curr. Appl. Phys.*, 2009, 9, pp. 224–226

[3] Wang W., Poudel B., Yang J., Wang D.Z., Ren Z.F.: 'High-yield synthesis of single-crystalline antimony telluride hexagonal nanoplates using a solvothermal approach', *J. Am. Chem. Soc.*, 2005, 127, pp. 13792–13793

[4] Zhou B., Ji Y., Yang Y.F., Li X.H., Zhu J.J.: 'Rapid microwave-assisted synthesis of single-crystalline Sb_2Te_3 hexagonal nanoplates', *Cryst. Growth Des.*, 2008, 8, pp. 4394–4397

[5] Shi W., Yu J., Wang H., Zhang H.: 'Hydrothermal synthesis of single-crystalline antimony telluride nanobelts', *J. Am. Chem. Soc.*, 2006, 128, pp. 16490–16491

[6] Bhunia S., Bose D.N.: 'Microwave synthesis, single crystal growth and characterization of ZnTe', *J. Cryst. Growth*, 1998, 186, pp. 535–542

[7] Lekse J.W., Pischera A.M., Aitken J.A.: 'Understanding solid-state microwave synthesis using the diamond-like semiconductor, AgInSe2, as a case study', *Mater. Res. Bull.*, 2007, 42, pp. 395–403

[8] Powder Diffract. File, JCPDS-ICDD, 12 Campus Boulevard, Newtown Square, PA 19073-3273, USA, 2001

[9] Suryanarayana C., Norton M.G.: 'X-ray diffraction, a practical approach' (Plenum Press, NY, 1998)

[10] Zheng B., Xiao Z., Chhay B., Zimmerman R.L., Edwards M.E., Ila D.: 'Thermoelectric properties of MeV Si ion bombarded Bi_2Te_3/Sb_2Te_3 superlattice deposited by magnetron sputtering', *Surf. Coat. Technol.*, 2009, 203, pp. 2682–2686

[11] Andrews K.W., Dyson D.J., Keown S.R.: 'Interpretation of electron diffraction patterns' (Plenum Press, New York, 1971)

[12] Garje S.S., Eisler D.J., Ritch J.S., Afzaal M., O'Brien P., Chivers T.: 'A new route to antimony telluride nanoplates from a single-source precursor', *J. Am. Chem. Soc.*, 2006, 128, pp. 3120–3121

[13] Jin C., Zhang G., Qian T., Li X., Yao Z.: 'Large-area Sb_2Te_3 nanowire arrays', *J. Phys. Chem. B*, 2005, 109, pp. 1430–1432

[14] Zuev Y.M., Lee J.S., Galloy C., Park H., Kim P.: 'Diameter dependence of the transport properties of antimony telluride nanowires', *Nano Lett.*, 2010, 10, pp. 3037–3040

[15] Rawat R.S., Arun P., Vedeshwar A.G., *ET AL.*: 'Effect of argon ion irradiation on Sb_2Te_3 films in a dense plasma focus device', *Mater. Res. Bull.*, 2000, 35, pp. 477–486

[16] Arun P., Vedeshwar A.G.: 'Influence of grain size on the electrical properties of Sb_2Te_3 polycrystalline films', *Mater. Res. Bull.*, 2003, 38, pp. 1929–1938

[17] Lee J.S., Brittman S., Yu D., Park H.: 'Vapor–liquid–solid and vapor–solid growth of phase-change Sb_2Te_3 nanowires and Sb_2Te_3/GeTe nanowire heterostructures', *J. Am. Chem. Soc.*, 2008, 130, pp. 6252–6258

[18] Tsunekawa S., Fukuda T., Kasuya A.: 'Blue shift in ultraviolet absorption spectra of monodisperse CeO_{2-x} nanoparticles', *J. Appl. Phys.*, 2000, 87, pp. 1318–1321

[19] Chen G.Y., Zhang W.X., Xu A.W.: 'Synthesis and characterization of single-crystal Sb_2S_3 nanotubes via an EDTA-assisted hydrothermal route', *Mater. Chem. Phys.*, 2010, 123, pp. 236–240

[20] Zhu Q.A., Gong M., Zhang C., Yong G.B., Xiang S.: 'Preparation of Sb_2S_3 nanomaterials with different morphologies via a refluxing approach', *J. Cryst. Growth*, 2009, 311, pp. 3651–3655

[21] Erdoğan İ.Y., Demir Ü.: 'Synthesis and characterization of Sb_2Te_3 nanofilms via electrochemical co-deposition method', *J. Electroanalyst. Chem.*, 2009, 633, pp. 253–258

[22] Yang J., Zhu W., Gao X., *ET AL.*: 'Formation and characterization of Sb_2Te_3 nanofilms on Pt by electrochemical atomic layer epitaxy', *J. Phys. Chem. B*, 2006, 110, pp. 4599–4604

CURRICULUM VITAE

Name Mr. Tawat Suriwong

Date of Birth October 24, 1980

Education

2004 - 2007 M.Eng (Chemical Engineering); Department of Chemical Engineering, Faculty of Engineering, Kasetsart University, Thailand

Thesis Title: Transesterification of Jatropha Curcas Linn. Oil Using Heterogeneous Catalysts: SO_4^{2-}/ZrO_2, $CaSO_4.2H_2O$ and $FeSO_4.7H_2O$

Thesis advisor: Assoc. Prof. Dr. Apinya Duangchan

1999-2003 BSc. (Chemistry), 2nd Class Honor; Department of Chemistry, Faculty of Science, Naresuan University, Thailand

Senior Project: Synthesis of Zinc Compounds used for Solar Cell Production.

Scholarships

2008 – Present The Royal Golden Jubilee Ph.D. Program of Thailand Research Found, Thailand.

2004 – 2007 Asian Development Bank (ADB), Research and Development Institute (KURDI, Kasetsart University

Experience

2010 Research fellow in the Future Resource, Energy, and Eco materials (FREE), Graduate School of Engineering, Osaka University, Japan (June –December, 2010)

Conference Participations

(1). The 3rd International Symposium on Functional Materials (ISFM2009), Jinju, Korea. "Solid-state synthesis of cubic ZnTe nanocrystals using a microwave plasma" on June 15-18, 2009.

(2). RGJ Seminar Series LXII, Biodiversity, Utilization and Global Warming Solution, Chiang Mai, Thailand. Solid-state synthesis of cubic ZnTe nanocrystals using a microwave plasma" on September 16, 2009

(3). The 3rd International Nanoelectronics Conference (INEC 2010), Hongkong. "Solid-state microwave induced plasma synthesis of antimony telluride" on January 3-8, 2010.

(4). The 3rd International Congress on Ceramics (ICC3), Osaka, Japan. on November 14-18, 2010.

(5). RGJ Seminar Series LXXIX, Recent Advances in Natural Product, Pharmaceutical, Food, Cosmetic and Environmental Sciences, "Solid-state microwave induced plasma synthesis of antimony telluride" on February 11, 2011.

(6). RGJ-Ph.D. Congress XII, Pattaya, Thailand. "Solid-state synthesis of cubic ZnTe nanocrystals using a microwave plasma" on April 1-3, 2011.

Journal Publications

(1). Tawat Suriwong, Somchai Thongtem, Titipun Thongtem, "Solid-state synthesis of cubic ZnTe nanocrystals using a microwave plasma", *Materials Letters*, 63 (2009) 2103-2106, doi:10.1016/j.matlet.2009.07.002.

(2). Tawat Suriwong, Ken Kurosaki, Somchai Thongtem, Adul Harnwunggmoung, Tohru Sugahara, Theerayuth Plirdpring, Yuji Ohishi, Hiroaki Muta, and Shinsuke Yamanaka, "Synthesis and high-temperature thermoelectric properties of Ni_3GaSb and Ni_3InSb", *Journal of Alloys and Compounds*, 509 (2011) 4014–4017, doi:10.1016/j.jallcom.2011.01.006.

(3). Tawat Suriwong, Titipun Thongtem, Somchai Thongtem, "Direct energy gap of Sb_2Te_3 synthesized by solid-state microwave plasma", *Micro & Nano Letters*, 6 (2011) 170-173, doi: 10.1049/mnl.2010.0227.

(4). Tawat Suriwong, Ken Kurosaki, Somchai Thongtem, Adul Harnwunggmoung, Tohru Sugahara, Theerayuth Plirdpring, Yuji Ohishi, Hiroaki Muta, and Shinsuke Yamanaka, "Synthesis and thermal conductivities of $ZnIn_2Te_4$ and $CdIn_2Te_4$ with defect-chalcopyrite structure", *Journal of Alloys and Compounds*, **xxx** (2011) xxxx–**xxxx**, doi:10.1016/j.jallcom.2011.04.086.